Cathepsin B modulates lysosomal biogenesis and host defense against *Francisella novicida* infection

Xiaopeng Qi,[1]* Si Ming Man,[1]* R.K. Subbarao Malireddi,[1] Rajendra Karki,[1] Christopher Lupfer,[1] Prajwal Gurung,[1] Geoffrey Neale,[2] Clifford S. Guy,[1] Mohamed Lamkanfi,[3,4] and Thirumala-Devi Kanneganti[1]

[1]Department of Immunology and [2]Hartwell Center for Bioinformatics and Biotechnology, St. Jude Children's Research Hospital, Memphis, TN 38105
[3]Inflammation Research Center, VIB, B-9052 Zwijnaarde-Ghent, Belgium
[4]Department of Internal Medicine, Ghent University, B-9000 Ghent, Belgium

Lysosomal cathepsins regulate an exquisite range of biological functions, and their deregulation is associated with inflammatory, metabolic, and degenerative diseases in humans. In this study, we identified a key cell-intrinsic role for cathepsin B as a negative feedback regulator of lysosomal biogenesis and autophagy. Mice and macrophages lacking cathepsin B activity had increased resistance to the cytosolic bacterial pathogen *Francisella novicida*. Genetic deletion or pharmacological inhibition of cathepsin B down-regulated mechanistic target of rapamycin activity and prevented cleavage of the lysosomal calcium channel TRPML1. These events drove transcription of lysosomal and autophagy genes via transcription factor EB, which increased lysosomal biogenesis and activation of autophagy initiation kinase ULK1 for clearance of the bacteria. Our results identified a fundamental biological function of cathepsin B in providing a checkpoint for homeostatic maintenance of lysosome populations and basic recycling functions in the cell.

INTRODUCTION

Lysosomes are cytoplasmic membrane–enclosed organelles filled with numerous acidic hydrolases. These organelles are dynamic and can fuse with a variety of vesicles to mediate degradation of extracellular materials that have been endocytosed or intracellular components that have been sequestered by autophagy. Furthermore, lysosomes are recycled and reformed after fusion with cargo-containing vacuoles (Luzio et al., 2007; Yu et al., 2010). Fundamental cellular processes orchestrated by lysosomes require cathepsin proteases; dysregulation of these activities contributes to the development of malignancy and Alzheimer's disease (Gocheva et al., 2006; Mueller-Steiner et al., 2006). Secretion of cathepsins from lysosomes is involved in lysosomal membrane permeabilization–mediated cell death via caspase-dependent and caspase-independent pathways (Kreuzaler et al., 2011; Aits and Jäättelä, 2013). In addition, lysosomal rupture and cytoplasmic release of cathepsin B triggered by phagocytosis of crystals lead to activation of the NLRP3 inflammasome and maturation of the proinflammatory cytokines IL-1β and IL-18, which are key events linked to the development of atherosclerosis and Alzheimer's disease (Halle et al., 2008; Duewell et al., 2010).

Certain lysosomal proteases also provide antimicrobial host defense against infection. Lysosomal acidic hydrolases, especially cathepsins, are executioner proteases used for degradation of intracellular bacteria within lysosomes. Macrophages lacking cathepsin D have a reduced capacity to kill bacteria during pneumococcal infection (Bewley et al., 2011). Similarly, mice with a genomic deletion of cathepsin E have increased susceptibility to infection by *Staphylococcus aureus* and *Porphyromonas gingivalis* (Tsukuba et al., 2006). Furthermore, a protective role for cathepsin L has been reported for *Mycoplasma pulmonis* infection (Xu et al., 2013). However, the relative contribution of different members within this large protease family in antibacterial host defense is largely underappreciated.

Here, we identified an important role for cathepsin B in driving increased susceptibility to the cytosolic pathogen *Francisella novicida* but not to the vacuolar-restricted pathogen *Salmonella enterica* serovar Typhimurium (*S.* Typhimurium). Genetic deletion or pharmacological inhibition of cathepsin B triggered signaling via down-regulation of mechanistic target of rapamycin (mTOR) and the lysosomal calcium channel TRPML1 to activate transcription factor EB (TFEB), which in turn results in increased lysosomal biogenesis and autophagy to mediate clearance of the bacteria. This phenomenon was not observed with genetic deletion of cathepsin G, elastase, or elastase and neutrophil

*X. Qi and S.M. Man contributed equally to this paper.

Correspondence to Thirumala-Devi Kanneganti: thirumala-devi.kanneganti@stjude.org

Abbreviations used: AMPK, adenosine monophosphate–activated protein kinase; CA-074 Me, CA-074 methyl ester; ERK, extracellular signal–regulated kinase; iNOS, inducible nitric oxide synthase; MOI, multiplicity of infection; MPO, myeloperoxidase; mTOR, mechanistic target of rapamycin; TFEB, transcription factor EB; TSB, tryptic soy broth.

The Rockefeller University Press $30.00
J. Exp. Med. 2016 Vol. 213 No. 10 2081–2097
www.jem.org/cgi/doi/10.1084/jem.20151938

proteinase 3. Our results, therefore, identified a fundamental negative regulatory function of cathepsin B in the host cell against *F. novicida* infection.

RESULTS

Cathepsin B negatively regulates host defense against *F. novicida* infection

Intracellularly replicating bacterial pathogens have evolved strategies to evade degradation by lysosomes to survive and replicate in the hostile environment of the host cell (Ray et al., 2009; Huang and Brumell, 2014). *F. novicida* escapes the vacuole to undergo replication in the cytoplasm of infected cells, whereas *S.* Typhimurium replicates inside *S. enterica*–containing vacuoles. Despite decades of research on cathepsin biology, the role of lysosomal cathepsins in host defense against intracellularly replicating bacterial pathogens with distinct intracellular lifestyles has remained enigmatic. To address this, WT mice and mice deficient in the lysosomal cathepsin B, cathepsin G, or the extralysosomal proteases elastase and neutrophil proteinase 3 were infected with *F. novicida* or *S.* Typhimurium, and survival was monitored over time. Mice of all genotypes succumbed with similar kinetics to *S.* Typhimurium infection with most animals dying within 8 d after infection (Fig. 1 A). In contrast, when infected with *F. novicida*, cathepsin B–deficient mice (*Ctsb*$^{-/-}$ mice) were significantly protected from lethality, with 65% of animals from this group surviving beyond day 10, compared with only 25% of WT mice (Fig. 1 B). Enhanced resistance to *F. novicida* infection was specific to *Ctsb*$^{-/-}$ mice because mice lacking cathepsin G, elastase, or elastase and neutrophil proteinase 3 died with similar kinetics as WT mice (Fig. 1 B).

Reduced mortality in *Ctsb*$^{-/-}$ mice could be caused by reduced bacterial burden. Therefore, we determined the number of bacteria in the spleen and liver of WT and *Ctsb*$^{-/-}$ mice after 1 and 3 d of infection with *F. novicida*. Bacterial loads in the liver and spleen of *Ctsb*$^{-/-}$ mice were significantly lower than those in WT mice on day 3 but not on day 1 after infection (Fig. 1, C and D). In agreement, less granulomas were formed in the liver of infected *Ctsb*$^{-/-}$ mice relative to WT controls (Fig. 1 E). Reduced bacterial burden of *Ctsb*$^{-/-}$ mice on day 3 after infection was also associated with reduced production of proinflammatory cytokines and chemokines in the liver (Fig. 1 F). Moreover, cell death and associated activation of the apoptotic caspases 3, 7, and 8 was diminished in the liver tissue of *Ctsb*$^{-/-}$ mice 3 d after infection (Fig. 1, G and H). These results suggested cathepsin B plays negative roles in host defense against *F. novicida* infection.

Intracellular growth of *F. novicida* is suppressed by the lack of cathepsin B

Recruitment of immune cells and production of proinflammatory cytokines are hallmarks of effective innate immune responses to infection (Cowley and Elkins, 2011). One possibility is that the improved early innate immune response in *Ctsb*$^{-/-}$ mice might restrict bacterial replication or increase bacterial killing and clearance. Therefore, we investigated the number of circulating total white blood cells, red blood cells, neutrophils, and monocytes in the blood of uninfected WT and *Ctsb*$^{-/-}$ mice and WT and *Ctsb*$^{-/-}$ mice infected with *F. novicida*. Relative to their uninfected controls, both WT and *Ctsb*$^{-/-}$ mice exhibited a global reduction in the numbers of circulating white blood cells (lymphocytes and myeloid cells) and monocytes and an increase in the number of neutrophils 24 h after *F. novicida* infection, whereas total red blood cell counts remained unchanged (Fig. 2 A). These results suggested that certain populations of circulating immune cells might have migrated from the BM to the sites of infection. However, no significant differences were noted in the prevalence of specific immune cell populations in circulation between infected WT and *Ctsb*$^{-/-}$ mice (Fig. 2 A). We also did not observe any difference in the number of CD11b^{+} Ly6g^{+} neutrophils and CD11b^{+} Ly6g^{-} monocyte populations in the liver and spleen of WT and *Ctsb*$^{-/-}$ mice 24 h after *F. novicida* infection when WT and *Ctsb*$^{-/-}$ mice have comparable bacterial burden in the liver and spleen (Fig. 2 B). Finally, the levels of the proinflammatory cytokines TNF, IL-1β, and IL-6 and the keratinocyte-derived chemokine (CXCL1) in liver and spleen of infected WT and *Ctsb*$^{-/-}$ mice were similar after 24 h of infection (Fig. 2 C), suggesting that cathepsin B controlled host defense against *F. novicida* independently of immune cell recruitment and cytokine or chemokine production.

Macrophages play a key role in controlling intracellular replication and dissemination of *F. novicida* (Hall et al., 2008). To investigate the role of cathepsin B in the control of *F. novicida* replication in macrophages, we infected primary BMDMs from WT and *Ctsb*$^{-/-}$ mice with *F. novicida* and determined the number of intracellular bacteria over time. Notably, *Ctsb*$^{-/-}$ BMDMs cleared bacteria more efficiently relative to WT BMDMs at 8 and 24 h after infection (Fig. 2 D). In agreement, inhibition of the cathepsin B protease activity with CA-074 methyl ester (Me) also enhanced the bactericidal activity of WT BMDMs (Fig. 2 E).

F. novicida infection in macrophages is detected by the DNA-sensing AIM2 inflammasome (Fernandes-Alnemri et al., 2010; Jones et al., 2010; Rathinam et al., 2010; Man et al., 2016), but cathepsin B was not required for AIM2-dependent activation of caspase 1, the subsequent release of the caspase 1 substrate IL-1β, and pyroptotic cell death in BMDMs infected with *F. novicida* (Fig. 3, A–C). Other members of the caspase family also contribute to innate immunity during infection (Man and Kanneganti, 2016). However, infected *Ctsb*$^{-/-}$ BMDMs displayed similar levels of caspases 3, 7, and 8 activation compared with infected WT BMDMs, in agreement with results from CA-074 Me–pretreated WT BMDMs (Fig. 3 D). Differential activation of apoptotic caspases was also not observed in liver tissues from WT and *Ctsb*$^{-/-}$ mice after 24 h of infection (Fig. 3 E).

Apart from inflammasome signaling, type I interferons, inducible nitric oxide synthase (iNOS), and antimicrobial

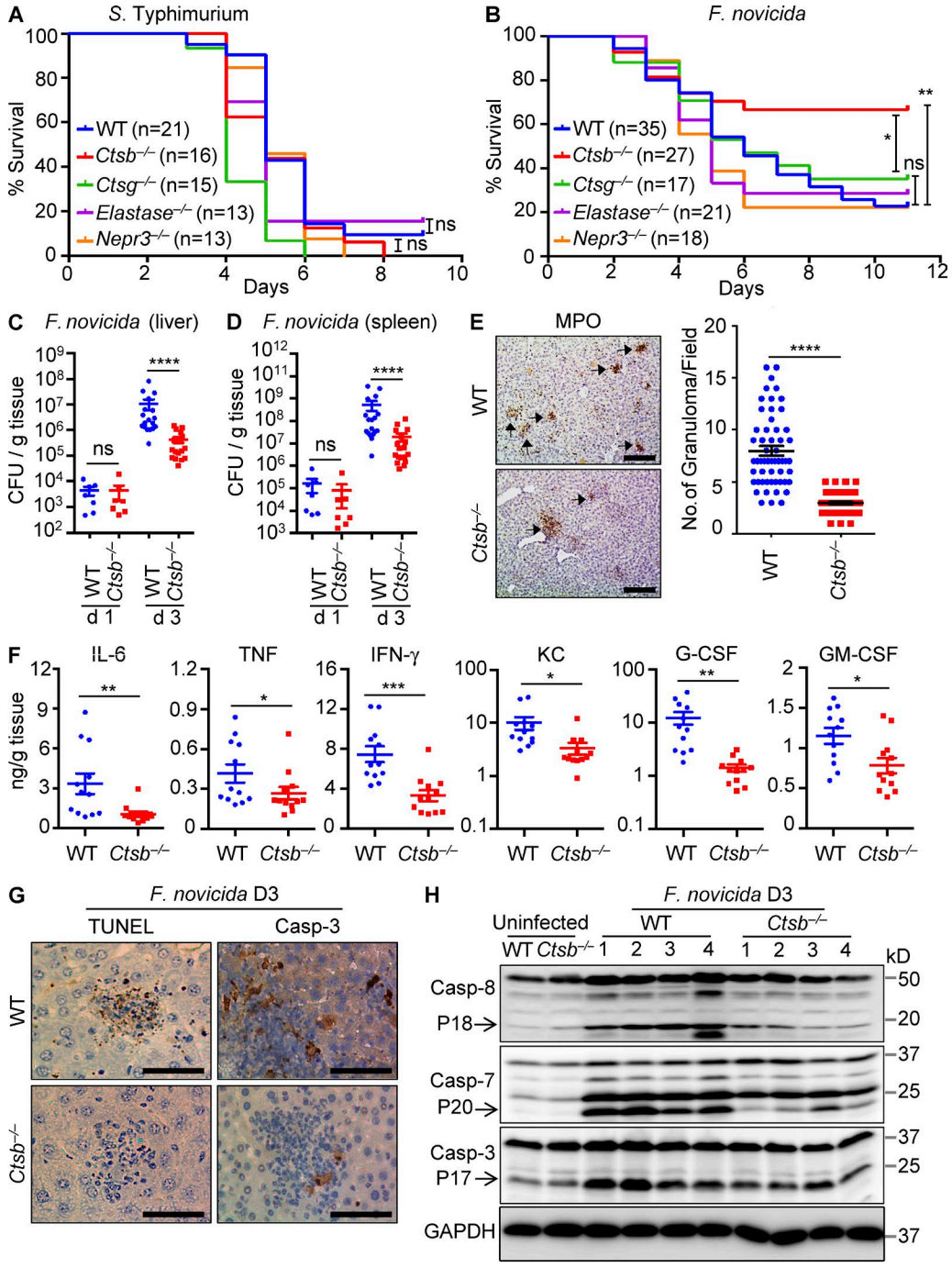

Figure 1. ***Ctsb*$^{-/-}$mice are resistant to *F. novicida* infection.** (A) WT and mutant mice were infected i.p. with 5×10^3 CFU of *S.* Typhimurium, and survival was monitored. (B) WT and mutant mice were infected subcutaneously with 1.5×10^5 CFU of *F. novicida*, and survival was monitored. (C and D) WT and *Ctsb*$^{-/-}$ mice were infected with 1.5×10^5 CFU of *F. novicida*. Bacterial burden in liver (C) and spleen (D) on days 1 and 3 was measured. (E) Liver sections from WT and *Ctsb*$^{-/-}$ mice infected with *F. novicida* (day 3) were stained with MPO. Quantification of MPO-stained granuloma and the number of granuloma per field are shown. (F) Proinflammatory cytokine and chemokine levels were measured in the liver from WT and *Ctsb*$^{-/-}$ mice on day 3 after infection with *F. novicida*. G-CSF, granulocyte CSF; KC, keratinocyte-derived chemokine. (G) TUNEL staining and cleaved caspase 3 (Casp-3) staining of liver sections from WT and *Ctsb*$^{-/-}$ mice after infection with *F. novicida* for 3 d (D3). (H) Liver tissue samples from WT and *Ctsb*$^{-/-}$ mice after infection with *F. novicida* for 3 d were homogenized, and lysates were analyzed for caspases 8, 3, and 7 activation by immunoblotting analysis. Each symbol indicates an individual mouse for C, D, and F. Data represent means ± SEM. Results are pooled from three independent experiments for A–D and are representative of two independent experiments for E–H. Bars, 100 µm. *, $P < 0.05$; **, $P < 0.01$; ***, $P < 0.001$; ****, $P < 0.0001$. ns, not significant.

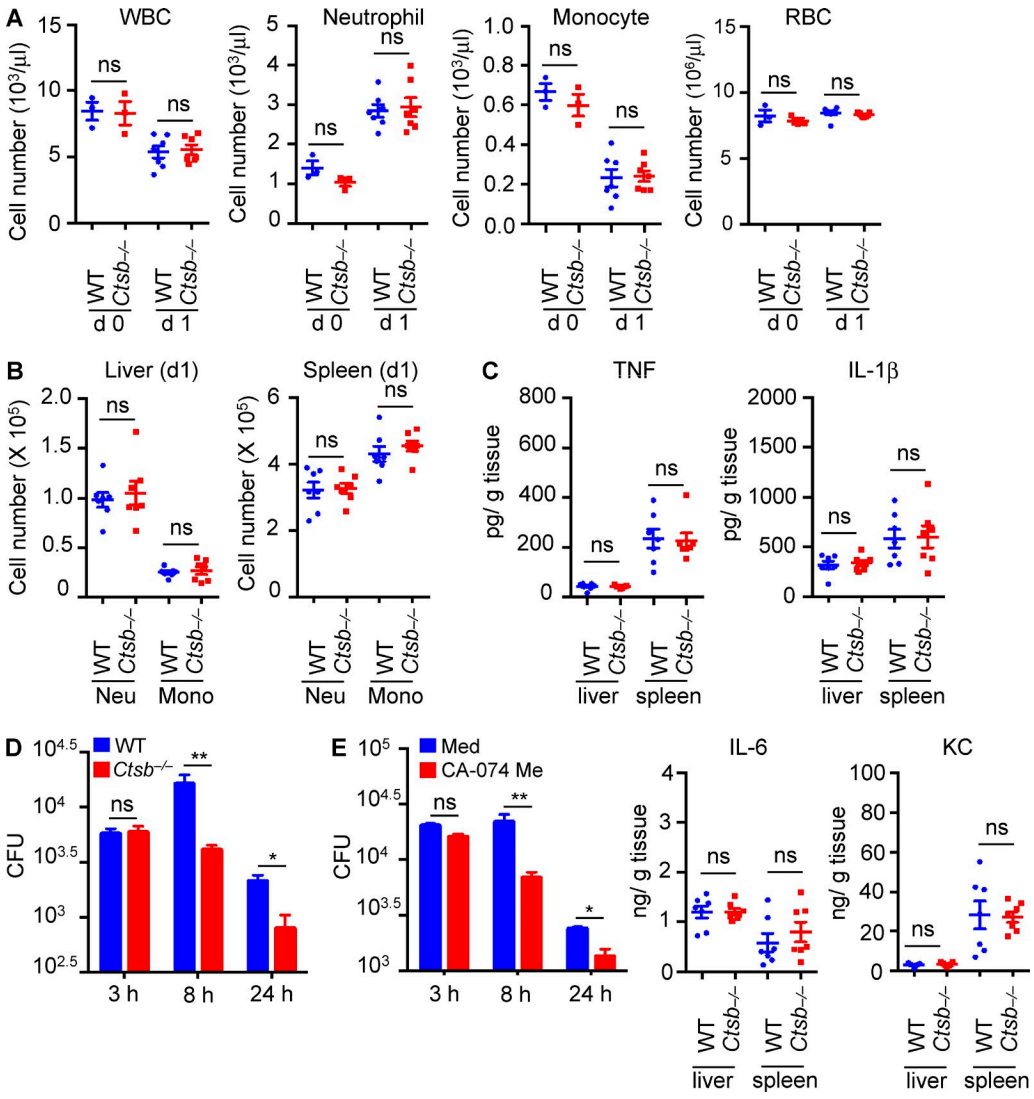

Figure 2. **Macrophages lacking cathepsin B have enhanced bactericidal activity.** (A) Blood cells from uninfected mice (d 0) or mice infected with *F. novicida* (d 1) were analyzed for different cell populations with a Forcyte hematology analyzer. WBC, white blood cell. (B) On day 1 after *F. novicida* infection, neutrophil ($CD11b^+$ $Ly6g^+$; Neu) and monocyte ($CD11b^+$ $Ly6g^-$; Mono) infiltration into the liver and spleen were analyzed. (C) Cytokine levels were measured in the liver and spleen from WT and $Ctsb^{-/-}$ mice on day 1 after infection with *F. novicida*. (D) BMDMs from WT and $Ctsb^{-/-}$ mice were infected with *F. novicida* (MOI 10) for 3 h, and numbers of intracellular bacteria were enumerated at the indicated times. (E) BMDMs from WT mice were infected with *F. novicida* (MOI 10) for 3 h in media (Med) with or without the cathepsin B inhibitor CA-074 Me (5 μM). The number of intracellular bacteria was enumerated at the indicated times. KC, keratinocyte-derived chemokine. Each symbol indicates an individual mouse and means ± SEM are shown. Data are representative of two independent experiments for A–C or three independent experiments for D and E. *, $P < 0.05$; **, $P < 0.01$. ns, not significant.

peptides regulate host protection against *F. novicida* infection (Lindgren et al., 2005; Henry et al., 2007). However, WT and $Ctsb^{-/-}$ BMDMs that have been infected with *F. novicida* expressed similar transcript levels of *Ifnb*, *iNos*, and the antimicrobial glycoprotein lipocalin 2 (*Lcn2*; Fig. 3 F). Also, the levels of activated NF-κB and extracellular signal–regulated kinase (ERK) as well as production of IL-6 and TNF were not differentially regulated in *F. novicida*–infected WT and $Ctsb^{-/-}$ BMDMs (Fig. 3, G and H). These data collectively suggested that the role of cathepsin B in the regulation of *F. novicida* replication is uncoupled from macrophage cell death, inflammasome activation, and inflammatory cytokine production.

Lysosomes target *F. novicida* in the absence of cathepsin B

Fusion of lysosomes with pathogen-occupied vacuoles is a major bactericidal mechanism in macrophages (Roy et al., 2006). In response, bacterial pathogens have evolved mechanisms to evade the lysosomal degradation pathway. During *F. novicida* infection, bacteria escape the vacuoles of human

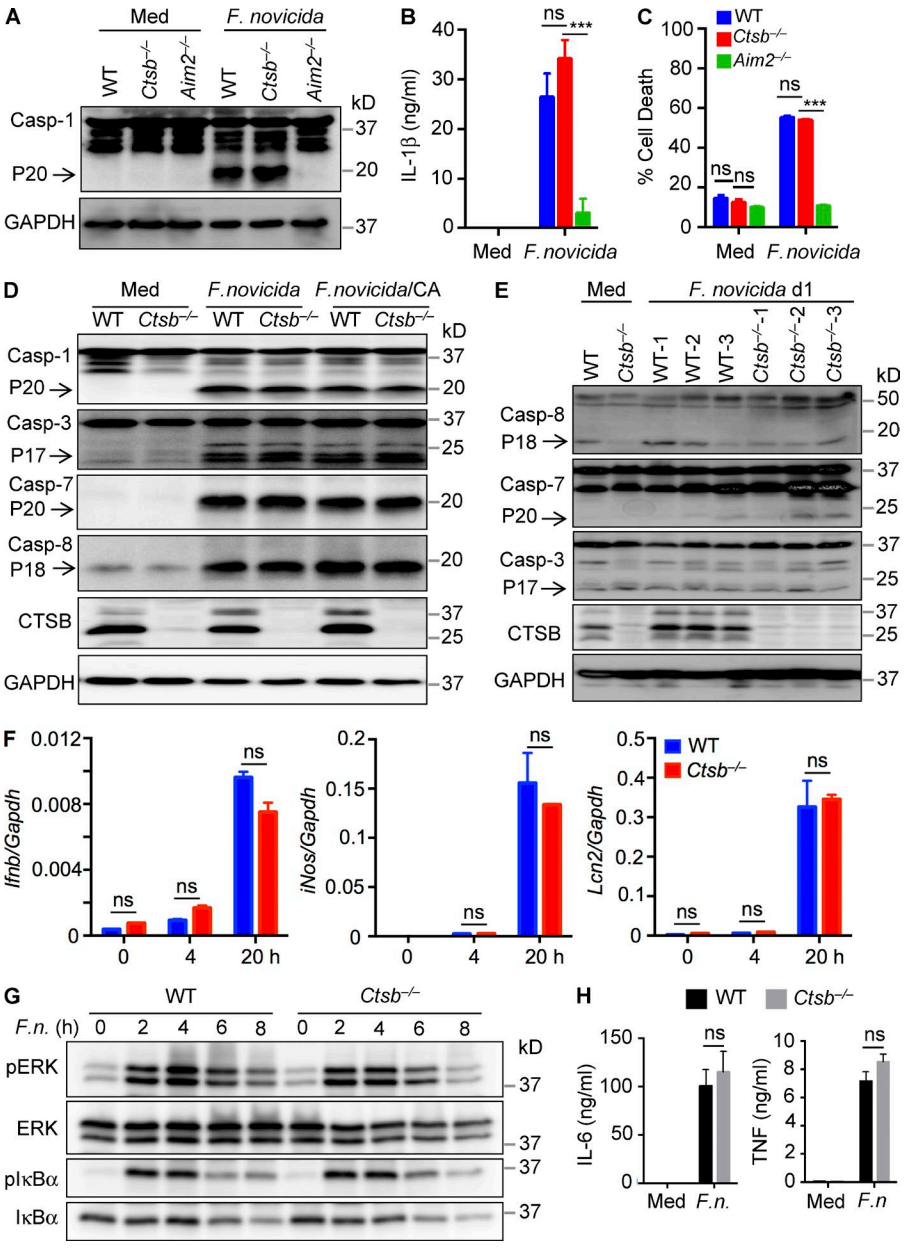

Figure 3. **Cathepsin B is dispensable for caspase activation and NF-κB and ERK signaling in response to *F. novicida* infection.** (A–C) Immunoblot analysis of caspase 1 (Casp-1) and its subunit P20 (A) and analysis of IL-1β release (B) and cell death (C) in WT, *Ctsb*$^{-/-}$, and *Aim2*$^{-/-}$ BMDMs infected with *F. novicida* (MOI 100) for 20 h. (D) Immunoblot analysis of caspases 1, 3, 7, and 8 in WT and *Ctsb*$^{-/-}$ BMDMs infected with *F. novicida* (MOI 100) for 20 h with or without 5 µM CA-074 Me (CA). Uninfected cells were used as negative controls. Arrows indicate the cleaved forms. (E) Liver homogenates from WT and *Ctsb*$^{-/-}$ mice after infection with *F. novicida* for 24 h were analyzed for caspases 8, 7, and 3 activation by immunoblotting analysis. Arrows indicate the cleaved forms. (F) Expression of the genes encoding IFN-β, iNOS, and Lcn2 was analyzed in WT and *Ctsb*$^{-/-}$ BMDMs infected with *F. novicida* for the indicated times by quantitative real-time PCR. (G) BMDMs from WT and *Ctsb*$^{-/-}$ mice were infected with *F. novicida* (MOI 100; *F.n.*) for the indicated times, and cell lysates were analyzed for phosphorylated and total ERK and IκBα proteins by immunoblotting analysis. (H) Production of IL-6 and TNF was detected in uninfected or *F. novicida*–infected WT and *Ctsb*$^{-/-}$ BMDMs. Data are representative of three independent experiments and are means ± SEM. ***, P < 0.001. Med, uninfected; ns, not significant.

macrophages after 3–4 h of infection (Santic et al., 2005; Clemens et al., 2009). To investigate whether improved control of *F. novicida* replication in the absence of cathepsin B was caused by increased fusion of *F. novicida*–containing vacuoles with lysosomes, we examined colocalization of a GFP-expressing strain of *F. novicida* with LysoTracker in infected WT and *Ctsb*$^{-/-}$ BMDMs. We found a significantly elevated frequency of *F. novicida* colocalizing with lysosomes in *Ctsb*$^{-/-}$ BMDMs compared with the numbers observed in WT BMDMs at 5 h (67.2 ± 1.8% vs. 51.1 ± 2.2%) and 12 h (94.8 ± 0.4% vs. 86.8 ± 0.9%) after infection (Fig. 4, A–D). These results suggested that the prevalence of lysosome-associated *F. novicida* increased in *Ctsb*$^{-/-}$ BMDMs compared with WT BMDMs. In agreement, treatment of WT BMDMs with a cathepsin B protease inhibitor CA-074 Me significantly increased the prevalence of LysoTracker-positive *F. novicida* (Fig. 4 E). Notably, we observed that *Ctsb*$^{-/-}$ BMDMs contained significantly more LysoTracker-positive vacuoles before infection, and the number of LysoTracker puncta in uninfected *Ctsb*$^{-/-}$ BMDMs was nearly twofold that of WT BMDMs (15.9 ± 0.5 vs. 8.3 ± 0.3 per cell; Fig. 4, F and G). The increased prevalence of LysoTracker-positive vacuoles and increased expression of the lysosomal membrane protein LAMP1 in *Ctsb*$^{-/-}$ BMDMs was further confirmed by flow cytometry and immunoblotting analysis, respectively (Fig. 4, H–K). Similar to *Ctsb*$^{-/-}$ BMDMs, the cathepsin B inhibitor CA-074 Me increased the number of LysoTracker puncta and expression of LAMP1 in WT BMDMs (Fig. 4, L–N).

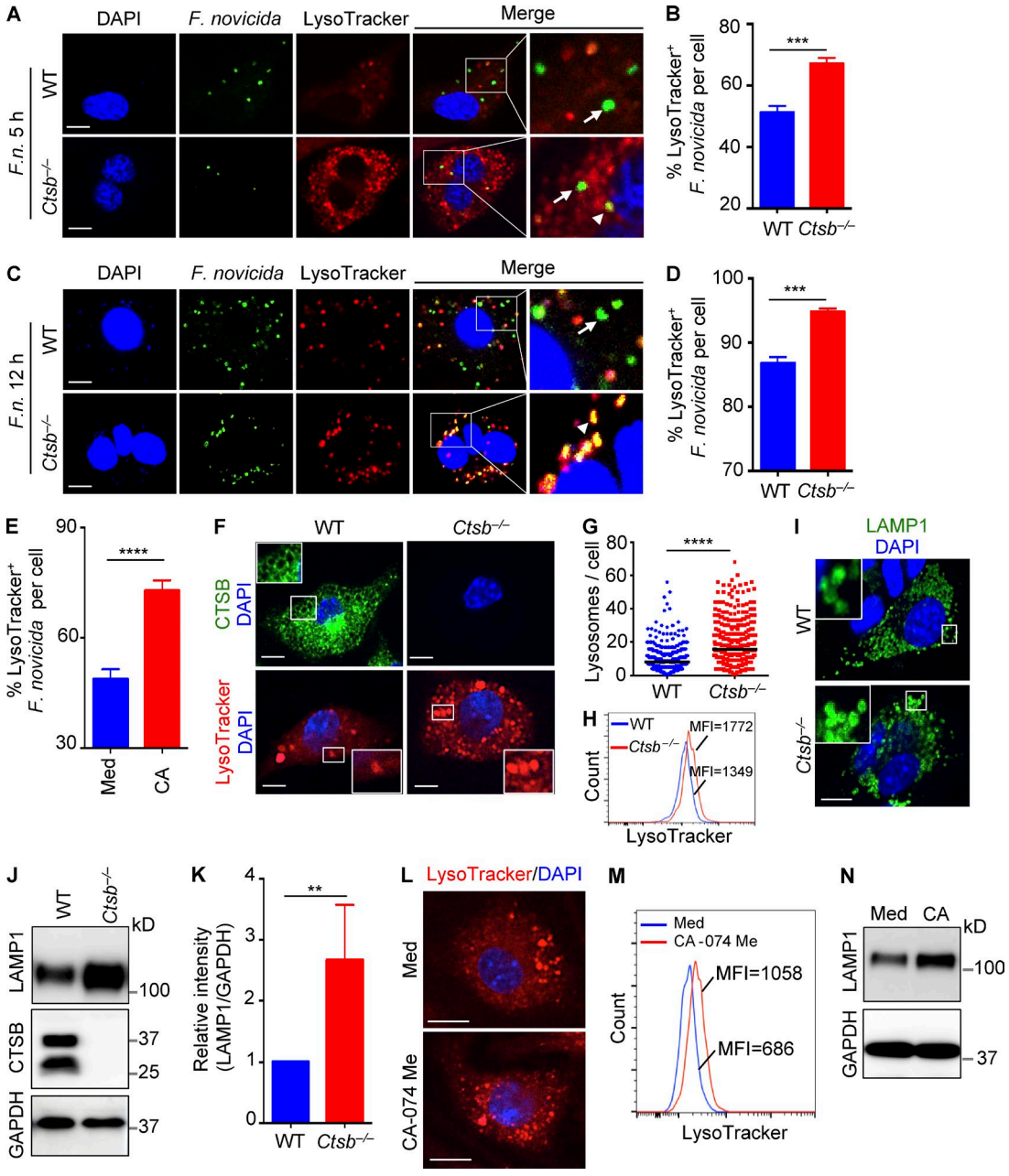

Figure 4. **Recruitment of the lysosome to *F. novicida* is accelerated in the absence of cathepsin B.** (A and C) BMDMs from WT and *Ctsb*$^{-/-}$ mice were infected with GFP-expressing *F. novicida* (MOI 20; *F.n.*) for 5 h (A) or 12 h (C) followed by labeling with 100 nM LysoTracker for 30 min. Fixed samples were processed for confocal microscopy. Arrowheads indicate lysosome-targeted *F. novicida*; arrows indicate *F. novicida* free from lysosome colocalization. (B and D) Quantification of A (B) and C (D) are shown. At least 220 cells were analyzed for each group. (E) Quantification of the percentage of *F. novicida* colocalized with lysosomes in WT BMDMs infected with GFP-expressing *F. novicida* (MOI 20) for 5 h in the presence or absence (Med) of 5 µM CA-074 Me (CA). At least 200 cells were analyzed for each group. (F) Confocal microscopy analysis of WT and *Ctsb*$^{-/-}$ BMDMs stained with cathepsin B antibody (top) or labeled with LysoTracker (bottom). Insets indicate enlarged images. (G) Quantification of lysosomes in WT and *Ctsb*$^{-/-}$ BMDMs. Each symbol indicates an individual cell. At least 500 cells were analyzed for each group. (H) FACS analysis of WT and *Ctsb*$^{-/-}$ BMDMs stained with LysoTracker. (I) Confocal microscopy showing LAMP1 staining in WT and *Ctsb*$^{-/-}$ BMDMs. Insets indicate enlarged images. (J) Cell lysates from WT and *Ctsb*$^{-/-}$ BMDMs were analyzed for LAMP1 protein expression by immunoblotting. (K) Quantification of the relative protein level of LAMP1 in J. (L) Representative images of WT BMDMs treated with or without cathepsin B inhibitor (5 µM CA-074 Me) for 12 h and labeled with LysoTracker. (M) FACS analysis of LysoTracker staining in WT BMDMs in the presence or absence of 5 µM CA-074 Me for 12 h. (N) Immunoblot analysis of LAMP1 expression in WT BMDMs in media or treated with 5 µM CA-074 Me for 12 h. Data are representative of three independent experiments and are means ± SEM. Bars, 10 µm. **, $P < 0.01$; ***, $P < 0.001$; ****, $P < 0.0001$. MFI, mean fluorescence intensity.

Transmission electron microscopy reveled that uninfected *Ctsb*$^{-/-}$ BMDMs contained larger single-membrane lysosomes and double-membrane autophagosomes compared with that in uninfected WT BMDMs (Fig. 5, A and C). Remarkably, higher resolution analysis of these micrographs revealed increased accumulation of partially digested vesicles in autolysosomes of *Ctsb*$^{-/-}$ BMDMs (Fig. 5 B), suggesting impaired nutrient recycling by *Ctsb*$^{-/-}$ lysosomes. Collectively, these results indicated that the enhanced antimicrobial activity of *Ctsb*$^{-/-}$ BMDMs to *F. novicida* might be attributed to their increased lysosomal biogenesis, which may result in increased efficiency in delivering the bacteria to lysosomes for killing.

Lysosomal biogenesis and autophagy are elevated in the absence of cathepsin B

We performed genome-wide expression analysis to profile differentially expressed genes in uninfected WT and *Ctsb*$^{-/-}$ BMDMs to examine whether the increased number of lysosomes in *Ctsb*$^{-/-}$ BMDMs is caused by enhanced lysosomal biogenesis. We identified increased expression of the gene encoding the TFEB and differentially regulated genes involved in the Coordinated Lysosomal Expression and Regulation (CLEAR) network as well as genes encoding lysosomal hydrolases, lysosomal membrane proteins, lysosomal acidification proteins, and autophagy proteins (Fig. 6 A and Fig. S1; Palmieri et al., 2011). Importantly, autophagy and lysosomal biogenesis in response to starvation signals are up-regulated by the CLEAR gene network and its regulatory transcription factor TFEB (Sardiello et al., 2009; Settembre et al., 2011). Consistent with the increased expression of TFEB mRNA, we found a substantial increase in the protein expression level of TFEB in uninfected *Ctsb*$^{-/-}$ BMDMs relative to those of WT controls (Fig. 6 B). Activated TFEB translocates into the nucleus to drive transcription of genes encoding lysosomal proteins containing the CLEAR element (Sardiello et al., 2009). We indeed observed increased nuclear localization of TFEB in *Ctsb*$^{-/-}$ BMDMs by immunofluorescence microscopy and immunoblotting analysis of TFEB (Fig. 6, C–E). These findings indicated that *Ctsb*$^{-/-}$ BMDMs have a superior capacity to drive lysosomal biogenesis by unleashing the activity of TFEB.

Activation and nuclear localization of TFEB are tightly regulated by signaling via mTOR (Settembre et al., 2012). Activated mTOR retains TFEB in the cytoplasm by inducing phosphorylation of TFEB, whereas inhibition of mTOR results in activation and nuclear translocation of TFEB. We investigated whether the mechanism of increased TFEB activation in the absence of cathepsin B was caused by down-regulated mTOR activation. Remarkably, phosphorylation of both mTOR and its direct target 4E-BP were significantly diminished in uninfected *Ctsb*$^{-/-}$ BMDMs compared with uninfected WT BMDMs (Fig. 6 F). We further confirmed this observation and found that WT BMDMs treated with CA-074 Me recapitulated the results obtained in *Ctsb*$^{-/-}$ BMDMs (Fig. 6 F).

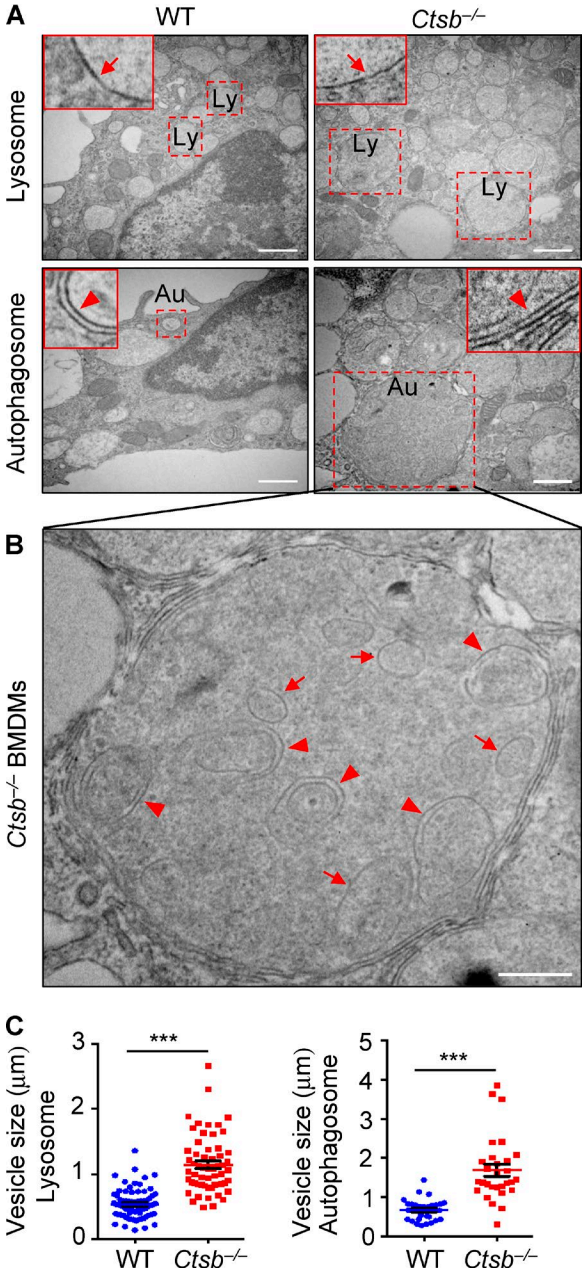

Figure 5. **Cathepsin B deficiency results in impaired lysosomal recycling.** (A) Transmission electron microscopy analysis of WT and *Ctsb*$^{-/-}$ BMDMs. Arrows in each inset indicate the single membrane lysosome- or double membrane autophagosome–associated vesicles. Dashed squares indicate a lysosome (Ly) or autophagosome (Au). (B) Undigested vesicles are accumulated in the autolysosomes of *Ctsb*$^{-/-}$ BMDMs. Arrows indicate double membrane–enclosed vesicles, and arrowheads indicate single membrane–enclosed vesicles. (C) Quantification of the size of lysosomes and autophagosomes from WT and *Ctsb*$^{-/-}$ BMDMs. The diameters of more than 60 lysosomes and 30 autophagosomes were analyzed. Data are representative of two independent experiments and are means ± SEM. Bars: (A) 1 μm; (B) 0.5 μm. ***, $P < 0.001$.

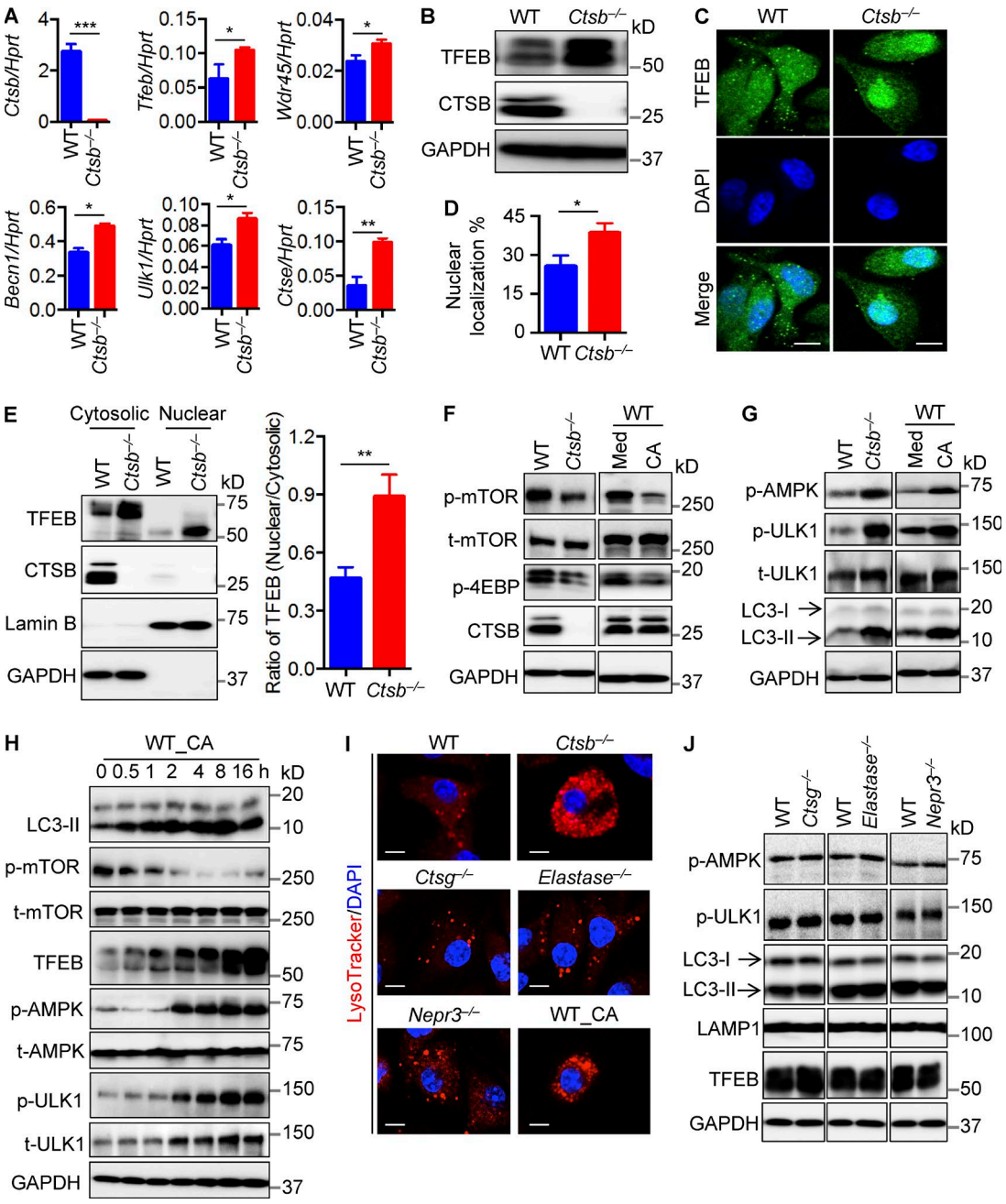

Figure 6. **Cathepsin B restricts lysosomal biogenesis and autophagy.** (A) Expression analysis of genes encoding cathepsin B, TFEB, WDR45, BECN1, ULK1, and cathepsin E in WT and *Ctsb*$^{-/-}$ BMDMs by quantitative real-time PCR. Ctse, cathepsin E; Hprt, hypoxanthine-guanine phosphoribosyltransferase. (B) Immunoblot analysis of TFEB, cathepsin B, and GAPDH (loading control) in uninfected WT and *Ctsb*$^{-/-}$ BMDMs. (C) Confocal microscopy analysis of TFEB staining in uninfected WT and *Ctsb*$^{-/-}$ BMDMs. (D) Percentage of nuclear localization of TFEB in uninfected WT and *Ctsb*$^{-/-}$ BMDMs. At least 200 cells were analyzed for each group. (E) Immunoblot analysis of TFEB in the nuclear and cytoplasmic fractions of uninfected WT and *Ctsb*$^{-/-}$ BMDMs (left) and the relative intensity of TFEB in nuclear versus cytoplasmic (right). Lamin B and GAPDH were used as quality controls for nuclear and cytoplasmic fractions separation, respectively. Quantification of the relative protein expression was processed using ImageJ. (F and G) Immunoblot analysis of phosphorylation of mTOR, 4EBP, AMPK, ULK1, and LC3-II in uninfected WT and *Ctsb*$^{-/-}$ BMDMs (left) or WT BMDMs in media (Med) with or without 5 µM CA-074 Me (CA) for 2 h. (H) Immunoblot analysis of proteins in F and G in WT BMDMs treated with 5 µM CA-074 Me for the indicated times. (I) Representative images of LysoTracker-labeled WT, *Ctsb*$^{-/-}$, *Ctsg*$^{-/-}$, *Elastase*$^{-/-}$, *Nepr3*$^{-/-}$, and cathepsin B inhibitor treated WT (WT_CA) BMDMs. (J) Immunoblot analysis of AMPK, ULK1, LC3, LAMP1, TFEB, and GAPDH (loading control) in uninfected WT, *Ctsg*$^{-/-}$, *Elastase*$^{-/-}$, and *Nepr3*$^{-/-}$ BMDMs. (C and I) Bars, 10 µm. Data are representative of three independent experiments and are means ± SEM. *, P < 0.05; **, P < 0.01; ***, P < 0.001. t-AMPK, total AMPK; t-mTOR, total mTOR.

Inhibition of mTOR is mediated by the conserved sensor of cellular energy and nutrient status, known as adenosine monophosphate–activated protein kinase (AMPK; Alers et al., 2012). AMPK also directly activates ULK1 to induce the autophagy pathway under stressed conditions (Kim et al., 2011). Notably, phosphorylation of both AMPK and ULK1 were substantially elevated in *Ctsb*$^{-/-}$ BMDMs (Fig. 6 G). Moreover, WT BMDMs treated with CA-074 Me phenocopied *Ctsb*$^{-/-}$ BMDMs (Fig. 6 G). To further confirm alterations in autophagy, we examined conversion of the autophagy marker LC3-I to the lipidated form of LC3-II. We indeed observed increased level of LC3-II in untreated *Ctsb*$^{-/-}$ BMDMs or in WT BMDMs treated with the cathepsin B inhibitor compared with untreated WT BMDMs (Fig. 6 G).

Next, we examined which pathway governed by mTOR, AMPK, and TFEB was the apical signal initiating the increase in lysosomal biogenesis and autophagy. A time course experiment assessing WT BMDMs treated with CA-074 Me showed that LC3-II accumulation and reduction of phosphorylated mTOR occurred within 30 min of cathepsin B inhibition (Fig. 6 H). In line with reduced phosphorylation of mTOR, the expression of TFEB was induced after treatment with the inhibitor for 30 min (Fig. 6 H). Phosphorylation of AMPK and ULK1 increased after 2 h of treatment with the cathepsin B inhibitor (Fig. 6 H), suggesting that AMPK and ULK1 activation succeeded LC3-II accumulation, reduction of phosphorylated mTOR, and activation of TFEB. These results suggested that impaired lysosomal degradation and recycling contributed to lysosomal biogenesis, whereas signaling via AMPK preferentially regulated the autophagy pathway and is not the apical signal driving increased lysosomal biogenesis in *Ctsb*$^{-/-}$ BMDMs. Importantly, we did not observe substantial differences in the number of lysosomes, phosphorylation of AMPK and ULK1, and protein expression of LC3-II, TFEB, and LAMP1 in *Cathepsin G*$^{-/-}$ (*Ctsg*$^{-/-}$), *Elastase*$^{-/-}$, or *Nepr3*$^{-/-}$ BMDMs compared with WT BMDMs (Fig. 6, I and J), suggesting that enhanced lysosomal biogenesis and autophagy are specific to *Ctsb*$^{-/-}$ BMDMs. Collectively, these results provided evidence to support that cathepsin B negatively regulated lysosomal biogenesis and autophagy at both the transcriptional and posttranslational levels through a mechanism that involved TFEB activation and ULK1 phosphorylation.

Cathepsin B down-regulates the TRPML1 channel activity in the lysosome

Lysosomal ion channels and transporters play essential roles in regulating signals from the lysosome (Xu and Ren, 2015). For instance, the vacuolar ATPase, a key player in lysosome nutrient sensing machinery, can sense lysosomal nutrient levels and regulate mTORC1 activity (Settembre et al., 2013). Calcium signaling mediated by the lysosomal calcium channel TRP ML1 (MCOLN1) regulates TFEB activity from the lysosome through the phosphatase calcineurin. Local calcineurin activation via TRPML1 is essential for nuclear translocation and activation of TFEB. The pathway regulating lysosomal biogenesis and autophagy seems to operate independently of mTOR (Medina et al., 2015). Previous studies have shown that cathepsin B mediates proteolytic cleavage of the lysosomal calcium flux channel TRPML1 (Kiselyov et al., 2005) and that a loss of TRPML1 induces leakage of cathepsin B into the cytoplasm (Colletti et al., 2012). It is possible that cathepsin B might mediate TRPML1 channel activity to regulate TFEB activity. Indeed, the protein level of the full-length TRPML1 was increased in *Ctsb*$^{-/-}$ BMDMs, whereas differential levels of the transcription of the gene encoding TRPML1 was not observed between untreated WT and *Ctsb*$^{-/-}$ BMDMs (Fig. 7, A and B), suggesting decreased cleavage of TRPML1 in *Ctsb*$^{-/-}$ BMDMs. We enriched lysosome fractions from BMDMs to investigate the level of TRPML1 cleavage. Cleavage of TRPML1 in the lysosome was substantially impaired in untreated *Ctsb*$^{-/-}$ BMDMs compared with untreated WT BMDMs (Fig. 7 C). We further examined whether an increased level of the full-length TRPML1 protein in *Ctsb*$^{-/-}$ BMDMs resulted in altered Ca^{2+} efflux from the lysosome. WT and *Ctsb*$^{-/-}$ BMDMs were treated with the TRPML1 agonist ML-SA1 (Shen et al., 2012). We observed increased Ca^{2+} release from the lysosome in *Ctsb*$^{-/-}$ BMDMs stimulated with ML-SA1 compared with treated WT BMDMs (Fig. 7 D). To further confirm whether lysosomal calcium signaling supported the increased TFEB activity in *Ctsb*$^{-/-}$ BMDMs, we treated *Ctsb*$^{-/-}$ BMDMs with the lysosomal TRPML1 inhibitor $PI(4,5)P_2$ (Zhang et al., 2012) and found that, over 8 h of inhibitor treatment, the expression of TFEB was substantially reduced in *Ctsb*$^{-/-}$ BMDMs (Fig. 7, E and F). Similar effects were observed in *Ctsb*$^{-/-}$ BMDMs treated with the calcineurin inhibitor cyclosporine A (Fig. 7, G and H). Collectively, these results suggested that cathepsin B negatively regulated TFEB activity, in part through lysosomal calcium signaling and degradation of TRPML1.

Autophagy is up-regulated in the absence of cathepsin B during *F. novicida* infection

Autophagy has been previously shown to mediate reentry of cytosolic-dwelling *F. novicida* to the endocytic pathway and fusion with lysosomes (Checroun et al., 2006). To investigate how cathepsin B modulates lysosomal biogenesis and autophagy during *F. novicida* infection, WT and *Ctsb*$^{-/-}$ BMDMs were infected with *F. novicida* and analyzed for $LC3^+$ puncta formation and TFEB expression. We found that *F. novicida* infection induced autophagy formation and significantly elevated the number of $LC3^+$ puncta per cell in *Ctsb*$^{-/-}$ BMDMs compared with infected WT BMDMs (Fig. 8, A and B). Moreover, the size of $LC3^+$ puncta in infected *Ctsb*$^{-/-}$ BMDMs was markedly increased relative to those observed in infected WT BMDMs (Fig. 8 C). Notably, the frequency of autophagosome-associated *F. novicida* was significantly higher in *Ctsb*$^{-/-}$ BMDMs than in WT BMDMs (Fig. 8 D). Furthermore, we found an increased frequency of nuclear-localized TFEB in *Ctsb*$^{-/-}$ BMDMs compared

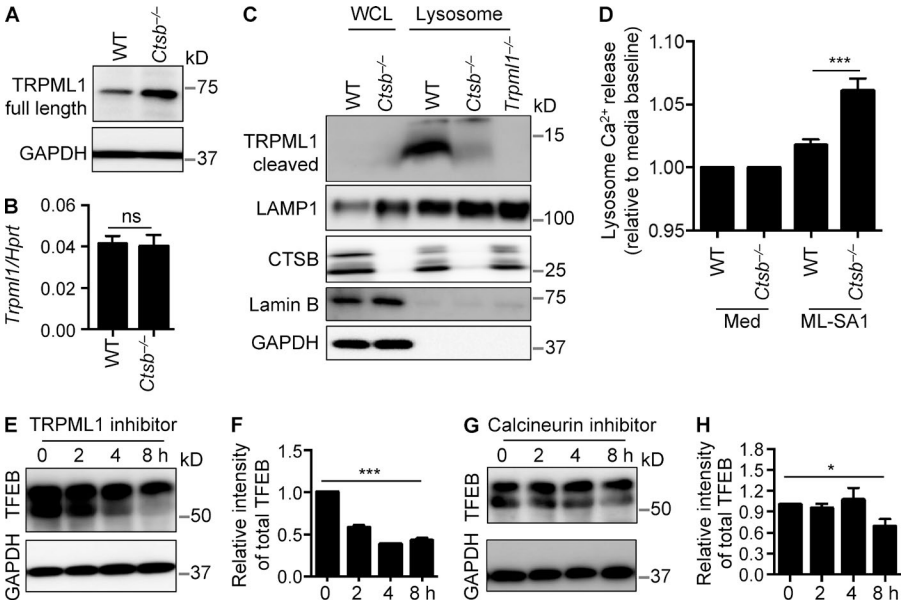

Figure 7. **Cathepsin B regulates TRPML1 channel activity.** (A) Immunoblot analysis of full-length TRPML1 in WT and *Ctsb*$^{-/-}$ BMDMs. (B) Quantitative real-time PCR analysis of *Trpml1* expression in WT and *Ctsb*$^{-/-}$ BMDMs. *Hprt*, hypoxanthine-guanine phosphoribosyltransferase; ns, not significant. (C) Immunoblot analysis of cleaved TRPML1 in the whole cell lysate (WCL) or lysosomes purified from WT, *Ctsb*$^{-/-}$, and immortalized *Trpml1*$^{-/-}$ BMDMs. LAMP1, cathepsin B, lamin B, and GAPDH were used as quality controls. (D) Lysosome calcium release was analyzed in WT and *Ctsb*$^{-/-}$ BMDMs stimulated with 20 µM ML-SA1. Med, media. (E) Immunoblot analysis of TFEB in *Ctsb*$^{-/-}$ BMDMs treated with 0.1 µM TRPML1 inhibitor $PI(4,5)P_2$ for the indicated times. (F) Quantification of data in E. (G) Immunoblot analysis of TFEB in *Ctsb*$^{-/-}$ BMDMs treated with 1 µM calcineurin inhibitor cyclosporin A for the indicated times. (H) Quantification of data in G. Data are representative of three independent experiments and are means ± SEM. *, $P < 0.05$; ***, $P < 0.001$.

with WT BMDMs after *F. novicida* infection (Fig. 8, E and F). Accordingly, both mRNA and protein levels of TFEB in infected *Ctsb*$^{-/-}$ BMDMs were higher than that of infected WT BMDMs (Fig. 8, G and H). We observed elevated phosphorylation of AMPK and ULK1 in *Ctsb*$^{-/-}$ BMDMs compared with their WT counterparts after *F. novicida* infection (Fig. 8, H and I). In line with the observation of increased phosphorylation of AMPK, the ratio of ADP to ATP in *Ctsb*$^{-/-}$ BMDMs was significantly higher than that of WT BMDMs after *F. novicida* infection (Fig. 8 J). Phosphorylated mTOR was further reduced in *Ctsb*$^{-/-}$ BMDMs infected with *F. novicida* (Fig. 8, H and I).

To further confirm that autophagy could play a protective role in the host defense against *F. novicida* infection, BMDMs from WT and autophagy-defective *Atg7*$^{-/-}$ mice (Martinez et al., 2011) were infected with *F. novicida* and analyzed for LC3 conversion and intracellular bacterial burden. Reduced LC3-II was observed in infected *Atg7*$^{-/-}$ BMDMs relative to infected WT BMDMs (Fig. 9, A and B), which was associated with increased numbers of *F. novicida* bacteria recovered from infected *Atg7*$^{-/-}$ BMDMs compared with the number recovered from infected WT BMDMs (Fig. 9 C).

To investigate whether the molecular mechanism orchestrated by cathepsin B to regulate autophagy and lysosomal biogenesis is recapitulated in a physiological setting, we analyzed signaling pathways in liver tissue homogenates from WT and *Ctsb*$^{-/-}$ mice. In agreement with our cellular analyses, uninfected *Ctsb*$^{-/-}$ mice or those infected with *F. novicida* exhibited a higher level of LC3-II compared with the corresponding WT controls (Fig. 9, D and E). Remarkably, LAMP1 expression was dramatically up-regulated in the liver of uninfected *Ctsb*$^{-/-}$ mice compared with uninfected WT mice, and both infected WT and *Ctsb*$^{-/-}$ mice maintained elevated levels of LAMP1 protein expression (Fig. 9 D). Moreover, expression of TFEB was significantly increased in *Ctsb*$^{-/-}$ mice (Fig. 9 F). In contrast, expression of *Lcn2*, a bacteriostatic factor produced during the innate immune response to bacterial infection, was similar in WT and *Ctsb*$^{-/-}$ mice after *F. novicida* infection (Fig. 9 F). Collectively, we identified a central role for cathepsin B in governing activities of TFEB and the kinase ULK1, resulting in suppression of lysosomal biogenesis and autophagy, respectively. Thus, the coordination of autophagy and lysosomal biogenesis induced by inhibition of cathepsin B facilitates host defense against *F. novicida* infection (Fig. 10).

DISCUSSION

Lysosomal cathepsins have been conventionally recognized as executive proteases for cargo degradation and cell death. Our study identified a central role for cathepsin B in governing activities of TFEB and the kinase ULK1, resulting in suppression of lysosomal biogenesis and autophagy, respectively. The involvement of cathepsin B in the lysosomal cell death pathway and activation of the NLRP3 inflammasome under certain physiological settings have attracted scientific interests (Tschopp and Schroder, 2010; Man and Kanneganti, 2015). Our results, however, indicated that genetic deletion of cathepsin B is dispensable for activation of the AIM2 inflammasome, cytokine production, and cell death typically associated with *F. novicida* infection (Henry et al., 2007; Fernandes-Alnemri et al., 2010; Jones et al., 2010; Rathinam et al., 2010; Man et al., 2015; Meunier et al., 2015), suggesting that there were additional roles of cathepsin B in host defense beyond inflammasome activation and cell death.

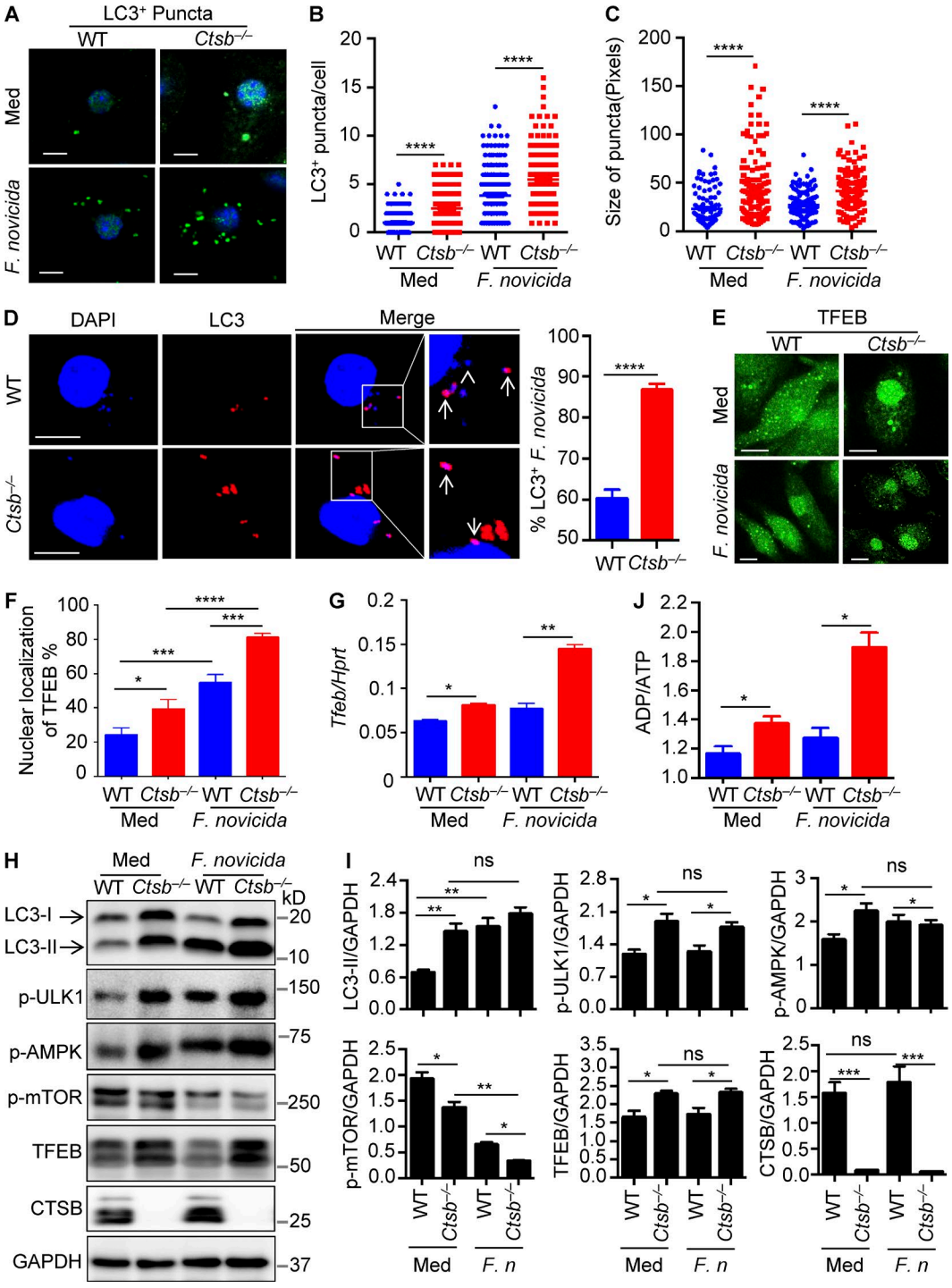

Figure 8. ***F. novicida* infection induces autophagy formation and TFEB activation in macrophages.** (A) Representative images of LC3-II⁺ puncta in uninfected (Med) WT and *Ctsb*$^{-/-}$ BMDMs or BMDMs infected with *F. novicida* for 4 h. (B) Quantification of the numbers of LC3-II⁺ puncta in WT and *Ctsb*$^{-/-}$ BMDMs with or without *F. novicida* infection. At least 200 cells were analyzed for each group. (C) Size of LC3-II⁺ puncta in WT and *Ctsb*$^{-/-}$ BMDMs in B. At least 100 cells were analyzed for each group. (D) Representative images of LC3-II⁺ puncta in WT and *Ctsb*$^{-/-}$ BMDMs infected with *F. novicida* for 4 h. Arrows indicate LC3-associated *F. novicida*; the arrowhead indicates LC3-II⁺ puncta free from *F. novicida* colocalization. At least 100 cells were analyzed in each group. (E) Confocal microscopy analysis of TFEB nuclear localization in WT and *Ctsb*$^{-/-}$ BMDMs with or without *F. novicida* infection. (F) Quantification of the percentage of TFEB nuclear localization. At least 200 cells were analyzed for each group. (G) Expression of the gene encoding TFEB was analyzed by quantitative real-time PCR. Hprt, hypoxanthine-guanine phosphoribosyltransferase. (H) Immunoblot analysis of LC3-II and TFEB and phosphorylation of ULK1, AMPK, and mTOR in uninfected WT and *Ctsb*$^{-/-}$ BMDMs or BMDMs infected with *F. novicida* for 3 h. (I) Quantification of the data in H. *F. n*, *F. novicida*;

In this study, we found a role for cathepsin B in negatively regulating lysosomal biogenesis and autophagy, such that cells lacking cathepsin B possessed a superior ability to induce fusion of their lysosomes with *F. novicida*. It is also interesting to speculate that *F. novicida* might be engulfed by autophagosomes and require cathepsin B to mediate entry to the cytoplasm for further replication. In addition, it is possible that the localization of cathepsin B proteins to a particular location within the host cell might contribute to their ability to influence the number of bacteria in the host cell.

We found that genomic deletion of cathepsin B in mice did not confer protection against the vacuolar-adapted pathogen *S.* Typhimurium, which could be because of differences in the mechanisms used by this bacterium to evade the lysosomal degradation pathway or to the functional redundancy among cathepsin proteases that are capable of inducing degradation of *S.* Typhimurium (Diacovich and Gorvel, 2010; Huang and Brumell, 2014). Further studies investigating the role of cytosolic pathogens, including both bacterial and viral pathogens, would yield insight into the biology of cathepsin B in infectious diseases. In particular, examining the effect of a range of doses of *F. novicida* infection in vivo would provide information on the strength of the impact of cathepsin B deletion (Nano et al., 2004; Kanistanon et al., 2012; Chu et al., 2014).

The role of autophagy in the host defense against members of the *Francisella* genus is controversial. The ability of different species or strains of the *Francisella* genus to evade the autophagy pathway might determine their intracellular survival (Chiu et al., 2009; Cremer et al., 2009; Chong et al., 2012; Steele et al., 2013). Results from the ATG7-deficient BMDMs from our study suggested that canonical autophagy is protective in the host defense against *F. novicida* infection. Lysosomes play critical roles in nutrient sensing and energy homeostasis (Settembre et al., 2013). During infection, neutralization of lysosomal pH by uropathogenic *Escherichia coli* in infected bladder epithelial cells can be sensed by the lysosomal cation channel TRPML3, subsequently triggering expulsion of exosome-encased bacteria (Miao et al., 2015). Our study now reveals a critical role of cathepsin B in controlling activity of the key lysosomal Ca^{2+} channel TRPML1. A lack of cathepsin B would leave the activity of TRPML1 unchecked, and a previous study has demonstrated that Ca^{2+} release by lysosomes via TRPML1 activates the phosphatase calcineurin, which, in turn, drives nuclear translocation of TFEB (Medina et al., 2015). Stressed signals from the lysosome itself might also inhibit mTOR activity and reduce phosphorylation of TFEB, leading to TFEB-dependent transcription of genes encoding molecules involved in lysosomal biogenesis and autophagy. The down-regulation of mTOR activity in *Ctsb*$^{-/-}$ BMDMs is consistent with a recent study showing that the mTORC1 pathway is activated by lysosomal degradation (Palm et al., 2015). It is not clear which specific signal elicited in the absence of cathepsin B down-regulated the phosphorylation of mTOR. However, enhanced AMPK phosphorylation in the absence of cathepsin B might provide a positive feedback reflecting increased lysosomal biogenesis, as this event occurred subsequent to TFEB and mTOR activation.

Our results unveiled a fundamental biological function of cathepsin B in providing a checkpoint for homeostatic maintenance of the lysosome population and basic recycling functions in the cell. Importantly, deficiency in cathepsin proteases causes lysosome storage diseases in humans owing to accumulation of partially digested macromolecules and enlarged lysosomes (Alroy and Lyons, 2014). TFEB-mediated lysosomal biogenesis and autophagy are crucial in exogenous antigen presentation and cancer metabolism (Perera et al., 2015; Samie and Cresswell, 2015). Cathepsin B can also mediate trypsinogen activation to promote the development of acute pancreatitis (van Acker et al., 2002). Our findings suggested that cathepsin B is a negative regulator of lysosomal biogenesis and autophagy in the intracellular milieu during a microbial infection, which broadens the biological repertoire of this protease in the context of health and disease. Our study, therefore, raises the intriguing possibility that modulating cathepsin B activity may hold therapeutic potential as a mean to increase host immunity against lethal *F. novicida* infection and to offer treatment options to those with debilitating lysosome storage diseases.

MATERIALS AND METHODS

Mice

WT C57BL/6J mice were purchased from The Jackson Laboratory and bred in house. *Ctsb*$^{-/-}$ mice were provided by T. Reinheckel (Albert-Ludwigs-University Freiburg, Freiburg, Germany), generated as described previously (Halangk et al., 2000), and backcrossed to the C57BL/6J background. *Ctsg*$^{-/-}$ (MacIvor et al., 1999) and *Nepr3*$^{-/-}$ (Kessenbrock et al., 2008) mice were provided by C. Pham (Washington University School of Medicine, St. Louis, MO). *Aim2*$^{-/-}$ (Jones et al., 2010) mice were provided by V.M. Dixit (Genentech, San Francisco, CA). LysM-Cre-*Atg7*$^{f/f}$ mice were described previously (Martinez et al., 2011). *Elastase*$^{-/-}$ mice were purchased from The Jackson Laboratory (stock no. 006112; Belaaouaj et al., 1998). All mutant mice were crossed with the C57BL/6J mice for >10 generations. All mice were kept in specific pathogen–free conditions within the Animal Resource Center at St. Jude Children's Research Hospital. Animal studies were conducted under protocols approved by the Institutional Animal Care and Use Committee of St. Jude Children's Research Hospital.

ns, not significant. (J) ADP to ATP ratio analysis in uninfected WT and *Ctsb*$^{-/-}$ BMDMs or BMDMs infected with *F. novicida* for 1 h. Data are representative of two independent experiments (A–D) or three independent experiments (E–J). Data represent means ± SEM. Bars, 10 µm. *, $P < 0.05$; **, $P < 0.01$; ***, $P < 0.001$; ****, $P < 0.0001$. ns, not significant.

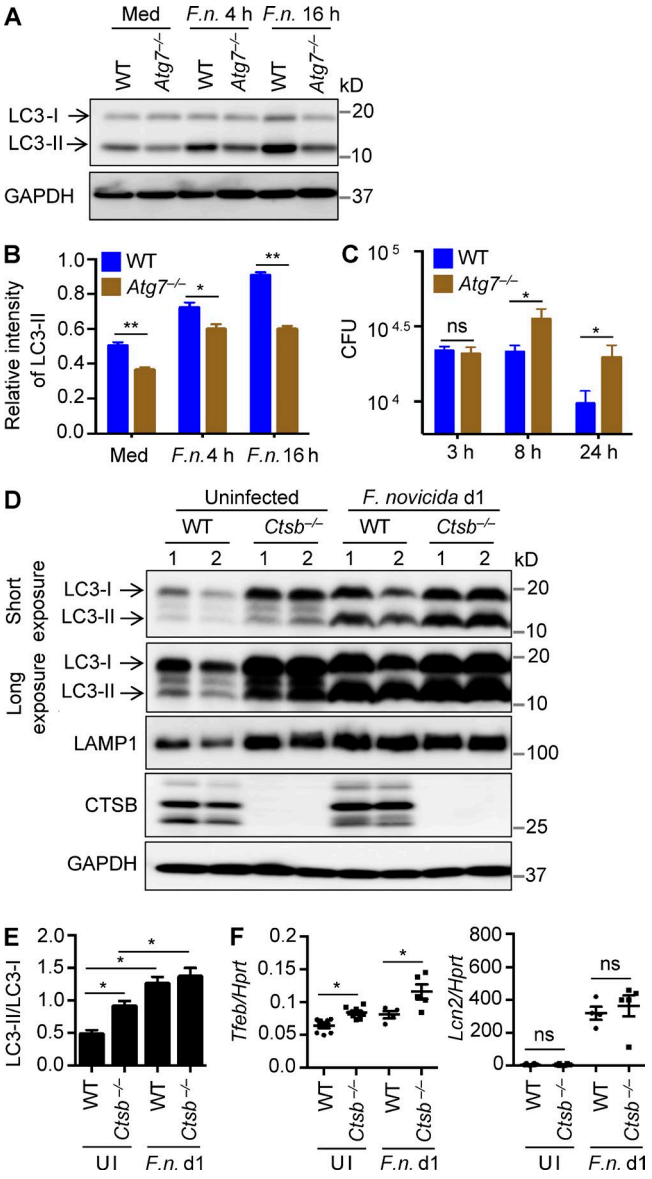

Figure 9. ***Ctsb*$^{-/-}$ mice have a greater capacity to induce autophagy and lysosomal biogenesis.** (A) Immunoblot analysis of LC3 in uninfected and *F. novicida* (*F.n.*)–infected WT and *Atg7*$^{-/-}$ BMDMs. (B) Quantification of data in A. (C) BMDMs from WT and LysM-Cre-*Atg7*$^{f/f}$ mice were infected with *F. novicida* (MOI 10) for 3 h, and numbers of intracellular bacteria were enumerated at the indicated times. (D) Immunoblot analysis of LC3, LAMP1, cathepsin B, and GAPDH (loading control) in liver homogenates of uninfected WT and *Ctsb*$^{-/-}$ mice and mice infected with *F. novicida* for 1 d. (E) Quantification of data for LC3-II conversion in D. (F) Expression of the genes encoding TFEB and LCN2 in the liver of uninfected mice and mice infected with *F. novicida* for 1 d. Data are representative of three independent experiments (A–C) or two independent experiments (D–F). Data represent means ± SEM. *, P < 0.05; **, P < 0.01. Hprt, hypoxanthine-guanine phosphoribosyltransferase; Med, media; ns, not significant; UI, uninfected.

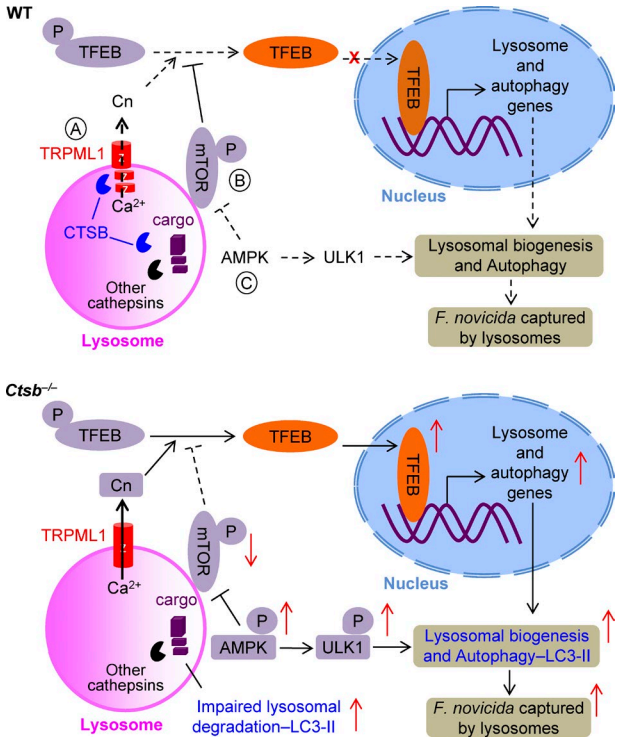

Figure 10. **A model of the regulation of lysosomal biogenesis and autophagy by cathepsin B in response to infection with *F. novicida*.** (A) Cathepsin B mediates cleavage of the TRPML1 channel and negatively regulates calcineurin (Cn) activity. (B) Deficiency in cathepsin B results in inhibition of mTOR activation owing to a stressed signal from the impaired lysosomal degradation. Both increased calcineurin and decreased mTOR activity in *Ctsb*$^{-/-}$ BMDMs drive nuclear translocation of TFEB, which in turn activates the transcription of genes associated with lysosome biogenesis and autophagy. (C) Stressed signals from the lysosome or a feedback signal from increased lysosomal biogenesis induces AMPK and ULK1 phosphorylation, which further activates the autophagy pathway. Thus, cathepsin B negatively regulates lysosomal biogenesis and autophagy at both the transcriptional and posttranslational levels. Increased lysosomal biogenesis and autophagy induced by cathepsin B deficiency results in effective clearance of the intracellular bacterial pathogen *F. novicida*. Red arrow, induced or reduced activity; black arrow, activation; black line with bar head, inhibition; solid line, activated; dash line, not activated.

Bacterial culture and infection of mice

The bacterial strains used in this study were *F. novicida* strain U112, GFP-expressing *F. novicida* (from D.M. Monack, Stanford University, Stanford, CA), and *S.* Typhimurium strain SL1344. *F. novicida* and *S.* Typhimurium were grown overnight with shaking in tryptic soy broth (TSB) and Luria-Bertani medium, respectively, subcultured for an additional 3–4 h, and resuspended in PBS. 8–10-wk-old mice were injected subcutaneously with *F. novicida* U112 (1.5×10^5 CFU per mouse) as described previously (Man et al., 2015). Mice were weighted and monitored daily over a period of 3 wk. Mice were euthanized at days 1 and 3 after infection,

and liver and spleen were harvested to determine the bacterial burden. Liver and spleen were homogenized, serially diluted, plated onto TSB agar plates, and incubated overnight at 37°C as described previously (Man et al., 2015). For *S.* Typhimurium infection, mice were infected i.p. with 5×10^3 CFU per mouse. For immune cell infiltration analysis, whole blood from WT and *Ctsb*$^{-/-}$ mice was analyzed on a hematology analyzer (Forcyte; Oxford Sciences) by a hematologist blinded to the experimental groups.

Bacterial infection of macrophages

To generate BMDMs, BM cells were cultured in L929 cell–conditioned IMDM supplemented with 10% FBS, 1% nonessential amino acids, and 1% penicillin-streptomycin for 5 d. Immortalized BM-derived cells from *Trpml1*$^{-/-}$ mice used for controls were from H. Fares (University of Arizona, Tucson, AZ; Miller et al., 2015). BMDMs were seeded in 12-well plates (1 million cells per well) and cultured overnight. The next day, cells were washed and supplied with fresh media without antibiotics. BMDMs were infected with *F. novicida* for the indicated times. For inhibitor treatment, BMDMs were treated with the cathepsin B inhibitor CA-074 Me (sc-214647; Santa Cruz Biotechnology, Inc.), AMPK inhibitor compound C (171260; EMD Millipore), calcineurin inhibitor cyclosporine A (PHR1092; Sigma-Aldrich), or lysosomal TRPML1 inhibitor PI(4,5)P_2 (R4504; Echelon Biosciences; Zhang et al., 2012). BMDMs were lysed in radioimmunoprecipitation assay buffer with protease and phosphatase inhibitors (Roche) for immunoblot analysis.

Bacterial killing assay

BMDMs were infected with *F. novicida* with a multiplicity of infection (MOI) of 10 for 2 h and washed, and 50 µg/ml gentamicin was added to kill extracellular bacteria. After 1 h, cells were washed twice and cultured in fresh media. BMDMs were lysed in sterile water at the indicated times after infection, serially diluted, plated onto TSB agar plates, and incubated overnight for CFU enumeration.

Preparation of liver sample for immunohistochemical staining and immunoblot analysis

Liver tissues were fixed in 10% formalin and embedded in paraffin for immunochemical staining. 4-µm–thick liver sections were stained with anti–cleaved caspase 3 or anti-myeloperoxidase (MPO) followed by incubation for 30 min with Rabbit-on-Rodent HRP polymer (RMR622; BioCare Medical). TUNEL (terminal deoxynucleotidyl transferase deoxyuridine triphosphate nick end labeling) staining was performed with the Dead End kit (G7130) according to the manufacturer's instructions (Promega). Liver tissues were homogenized in radioimmunoprecipitation assay buffer with protease and phosphatase inhibitors for immunoblot analysis. Protein concentrations were determined using a bicinchoninic acid assay kit (Thermo Fisher Scientific) according to manufacturer's instructions.

Immunoblot analysis and antibodies

Samples were separated by 12% SDS-PAGE and followed by electrophoretic transfer onto polyvinylidene fluoride membranes as described previously (Karki et al., 2015). Membranes were blocked with 5% nonfat milk and further incubated overnight in primary antibody at 4°C. The following primary antibodies were used: mouse IκBα, phosphorylated IκBα (p-IκBα; S32), ERK, p-ERK (T202Y204 [Cell signaling Technology], 9242L, 2859L, 9101L, and 9102L), anti–caspase 1 (AG-20B-0042; Adipogen), anti-LC3B (NB600-1384; Novus Biologicals), anti-LAMP1 (14-1071-85; eBioscience), antibodies for caspase 3, 7, and 8 (9661S, 9491S, and 8592S; Cell Signaling Technology), anti–cathepsin B (AF965; R&D Systems), antibodies for p-ULK1 (S555), total mTOR, p-mTOR (S2448), p–4E-BP1 (T37/46), total AMPK, p-AMPK (T172 [Cell Signaling Technology], 5869S, 2972S, 5536S, 2855P, 2793S, and 2535P), anti-ULK1 (A7481; Sigma-Aldrich), anti-TFEB (A303-673A; Bethyl Laboratories, Inc.), anti-TRPML1 (M1571; Sigma-Aldrich), anti-ATP6V1B2 (ab73404;Abcam), anti-MARCKS (myristoylated alanine-rich C kinase substrate; ab51100; Abcam), anti–lamin B (SC-6216; Santa Cruz Biotechnology, Inc.), and anti-GAPDH (5174S; Cell Signaling Technology). The secondary antibodies used were HRP-labeled anti–rabbit, anti–mouse, or anti–goat antibodies (Jackson ImmunoResearch Laboratories, Inc.). Quantification of the relative protein expression was processed using ImageJ (National Institutes of Health).

Immunofluorescence staining and microscopy

For LysoTracker staining and colocalization with *F. novicida*, WT and *Ctsb*$^{-/-}$ BMDMs were infected with GFP-expressing *F. novicida* and followed by labeling with 100 nM LysoTracker (L-7528; Molecular Probes) for the last 30 min. Cells were washed and fixed with 4% paraformaldehyde for 15 min at room temperature. Cells were washed three times and mounted using mounting medium (H-1200; Vector Laboratories). For LC3B, LAMP1, and TFEB immunostaining, uninfected and infected BMDMs were fixed in 4% paraformaldehyde for 15 min at room temperature. Cells were then permeabilized with cold methanol for 5 min, washed with PBS, and blocked in 1× ELISA buffer with 0.1% saponin for 1 h. Cells were stained with anti-LC3B (NB600-1384; Novus Biologicals), anti-LAMP1 (14-1071-85; eBioscience), or anti-TFEB (A303-673A; Bethyl Laboratories, Inc.), all at 1:500 dilution, overnight at 4°C. Cells were washed, stained with fluorescence-conjugated secondary antibody for 1 h, and mounted using mounting medium (H-1200; Vector Laboratories). Cells were observed on a confocal microscope (Axio Observer; Z1; SlideBook 6 software; ZEISS) for image acquisition and data analysis.

Transmission electron microscopy

BMDMs were fixed in 2% paraformaldehyde and 2.5% glutaraldehyde in 0.1 M cacodylate buffer (pH 7.4) for 1 h at 37°C. Cells were embedded and sectioned for transmission electron microscopy by the Cell and Tissue

Imaging Core Facility of St. Jude Children's Research Hospital. Quantification of lysosome and autophagosome size was performed with ImageJ.

Lysosome isolation

Lysosomes from BMDMs were isolated using a lysosome enrichment kit with cultured cell sonication and density gradient centrifugation, followed by lysosome precipitation according to the manufacturer's manual (89839; Thermo Fisher Scientific). The purity of isolated lysosomes was determined by detecting the lysosomal membrane protein LAMP1, luminal lysosomal protease cathepsin B, nuclear protein lamin B, and GAPDH using immunoblotting analysis.

Lysosome calcium release measurement

WT and *Ctsb*$^{-/-}$ BMDMs were labeled with a calcium indicator (O-6807; Thermo Fisher Scientific) in calcium-free media for 15 min. Calcium release from the lysosome induced by 20 μM ML-SA1 and 200 μM glycylphenylalanine 2-naphthylamide was analyzed according to fluorescence intensity at 488 nm recorded with a confocal imaging system as described previously (Shen et al., 2012).

ADP/ATP ratio assay

Both infected and uninfected WT and *Ctsb*$^{-/-}$ BMDMs were lysed in assay buffer, and ATP and ADP content were measured using an ADP/ATP ratio assay kit according to the manufacturer's protocols (MAK135; Sigma-Aldrich).

Microarray analysis

Total RNA was extracted from WT and *Ctsb*$^{-/-}$ BMDMs, reverse transcribed into biotin-labeled cRNA with an Ambion WT Expression kit (Thermo Fisher Scientific), and hybridized to a Mouse Gene 2.0 ST GeneChip (Affymetrix). Gene expression data were normalized and transformed into $\log_2$ transcript expression values with the robust multiarray average algorithm (version 6.6; Partek Genomics Suite; Irizarry et al., 2003). Differential expression was defined by application of a difference in expression of 0.5-fold ($\log_2$ signal) between conditions. The dataset has been deposited in the GEO database under accession no. GSE79508.

Lactate dehydrogenase release assay

Cell culture supernatants were collected at the indicated times, and lactate dehydrogenase activity was measured by using the Promega cytotoxicity kit according to the manufacturer's protocols.

ELISA

Cell culture supernatant or sera from mice were analyzed for cytokine and chemokine release using a 22-multiplex assay (EMD Millipore) following the manufacturer's instructions.

Real-time quantitative PCR

Total RNA was isolated from BMDMs using TRIzol (Invitrogen). cDNA was reverse transcribed by using Superscript III reverse transcriptase (Invitrogen). Real-time quantitative PCR was performed on the ABI Prism 7500 sequence detection system (Applied Biosystems). Primer sequences are listed in Table S1.

Statistical analysis

Data are given as means ± SEM. Statistical analyses were performed using one-way ANOVA with multiple comparisons, two-tailed Student *t* tests, and log-rank tests. P-values ≤ 0.05 were considered significant.

Online supplemental material

Fig. S1 shows the expression of genes encoding TFEB, and its targets are differentially regulated in the absence of cathepsin B. Table S1 shows real-time quantitative PCR primer sequences. Online supplemental material is available at http://www.jem.org/cgi/content/full/jem.20151938/DC1.

ACKNOWLEDGMENTS

We thank T. Reinheckel for the *Ctsb*$^{-/-}$ mice, C. Pham for *Ctsg*$^{-/-}$ and *Nepr3*$^{-/-}$ mice, V.M. Dixit for the *Aim2*$^{-/-}$ mice, D.M. Monack for GFP-expressing *F. novicida*, H. Fares for the immortalized *Trpml1*$^{-/-}$ cells, and M. Barr, R. Johnson, A. Burton, and S. Frase (St. Jude Children's Research Hospital) for technical assistance.

This work was supported by the US National Institutes of Health (AI101935, AI124346, AR056296, and CA163507 to T.-D. Kanneganti), the American Lebanese Syrian Associated Charities (grant to T.-D. Kanneganti), the European Research Council (281600 to M. Lamkanfi), the Fund for Scientific Research-Flanders (G030212N to M. Lamkanfi), and the National Health and Medical Research Council of Australia (R.G. Menzies Early Career Fellowship APP1091544 to S.M. Man).

The authors declare no competing financial interests.

Author contributions: X. Qi, S.M. Man, and T.-D. Kanneganti designed the study; X. Qi, S.M. Man, R.K.S. Malireddi, R. Karki, C. Lupfer, P. Gurung, C.S. Guy, and G. Neale performed experiments and analyzed the data; and X. Qi, S.M. Man, M. Lamkanfi, and T.-D. Kanneganti wrote the manuscript.

Submitted: 13 December 2015
Accepted: 22 July 2016

REFERENCES

Aits, S., and M. Jäättelä. 2013. Lysosomal cell death at a glance. *J. Cell Sci.* 126:1905–1912. http://dx.doi.org/10.1242/jcs.091181

Alers, S., A.S. Löffler, S. Wesselborg, and B. Stork. 2012. Role of AMPK-mTOR-Ulk1/2 in the regulation of autophagy: cross talk, shortcuts, and feedbacks. *Mol. Cell. Biol.* 32:2–11. http://dx.doi.org/10.1128/MCB.06159-11

Alroy, J., and J.A. Lyons. 2014. Lysosomal storage diseases. *Journal of Inborn Errors of Metabolism & Screening.* 79:619–636. http://dx.doi.org/10.1134/S0006297914070049

Belaaouaj, A., R. McCarthy, M. Baumann, Z. Gao, T.J. Ley, S.N. Abraham, and S.D. Shapiro. 1998. Mice lacking neutrophil elastase reveal impaired host defense against gram negative bacterial sepsis. *Nat. Med.* 4:615–618. http://dx.doi.org/10.1038/nm0598-615

Bewley, M.A., H.M. Marriott, C. Tulone, S.E. Francis, T.J. Mitchell, R.C. Read, B. Chain, G. Kroemer, M.K.B. Whyte, and D.H. Dockrell. 2011. A cardinal role for cathepsin D in co-ordinating the host-mediated

apoptosis of macrophages and killing of pneumococci. *PLoS Pathog.* 7:e1001262. http://dx.doi.org/10.1371/journal.ppat.1001262

Checroun, C., T.D. Wehrly, E.R. Fischer, S.F. Hayes, and J. Celli. 2006. Autophagy-mediated reentry of *Francisella tularensis* into the endocytic compartment after cytoplasmic replication. *Proc. Natl. Acad. Sci. USA.* 103:14578–14583. http://dx.doi.org/10.1073/pnas.0601838103

Chiu, H.-C., S. Soni, S.K. Kulp, H. Curry, D. Wang, J.S. Gunn, L.S. Schlesinger, and C.-S. Chen. 2009. Eradication of intracellular *Francisella tularensis* in THP-1 human macrophages with a novel autophagy inducing agent. *J. Biomed. Sci.* 16:110. http://dx.doi.org/10.1186/1423-0127-16-110

Chong, A., T.D. Wehrly, R. Child, B. Hansen, S. Hwang, H.W. Virgin, and J. Celli. 2012. Cytosolic clearance of replication-deficient mutants reveals *Francisella tularensis* interactions with the autophagic pathway. *Autophagy.* 8:1342–1356. http://dx.doi.org/10.4161/auto.20808

Chu, P., A.L. Cunningham, J.J. Yu, J.Q. Nguyen, J.R. Barker, C.R. Lyons, J. Wilder, M. Valderas, R.L. Sherwood, B.P. Arulanandam, and K.E. Klose. 2014. Live attenuated *Francisella novicida* vaccine protects against *Francisella tularensis* pulmonary challenge in rats and non-human primates. *PLoS Pathog.* 10:e1004439. http://dx.doi.org/10.1371/journal.ppat.1004439

Clemens, D.L., B.-Y. Lee, and M.A. Horwitz. 2009. *Francisella tularensis* phagosomal escape does not require acidification of the phagosome. *Infect. Immun.* 77:1757–1773. http://dx.doi.org/10.1128/IAI.01485-08

Colletti, G.A., M.T. Miedel, J. Quinn, N. Andharia, O.A. Weisz, and K. Kiselyov. 2012. Loss of lysosomal ion channel transient receptor potential channel mucolipin-1 (TRPML1) leads to cathepsin B-dependent apoptosis. *J. Biol. Chem.* 287:8082–8091. http://dx.doi.org/10.1074/jbc.M111.285536

Cowley, S.C., and K.L. Elkins. 2011. Immunity to *Francisella*. *Front. Microbiol.* 2:26. http://dx.doi.org/10.3389/fmicb.2011.00026

Cremer, T.J., A. Amer, S. Tridandapani, and J.P. Butchar. 2009. *Francisella tularensis* regulates autophagy-related host cell signaling pathways. *Autophagy.* 5:125–128. http://dx.doi.org/10.4161/auto.5.1.7305

Diacovich, L., and J.-P. Gorvel. 2010. Bacterial manipulation of innate immunity to promote infection. *Nat. Rev. Microbiol.* 8:117–128. http://dx.doi.org/10.1038/nrmicro2295

Duewell, P., H. Kono, K.J. Rayner, C.M. Sirois, G. Vladimer, F.G. Bauernfeind, G.S. Abela, L. Franchi, G. Nuñez, M. Schnurr, et al. 2010. NLRP3 inflammasomes are required for atherogenesis and activated by cholesterol crystals. *Nature.* 464:1357–1361. http://dx.doi.org/10.1038/nature08938

Fernandes-Alnemri, T., J.W. Yu, C. Juliana, L. Solorzano, S. Kang, J. Wu, P. Datta, M. McCormick, L. Huang, E. McDermott, et al. 2010. The AIM2 inflammasome is critical for innate immunity to *Francisella tularensis*. *Nat. Immunol.* 11:385–393. http://dx.doi.org/10.1038/ni.1859

Gocheva, V., W. Zeng, D. Ke, D. Klimstra, T. Reinheckel, C. Peters, D. Hanahan, and J.A. Joyce. 2006. Distinct roles for cysteine cathepsin genes in multistage tumorigenesis. *Genes Dev.* 20:543–556. http://dx.doi.org/10.1101/gad.1407406

Halangk, W., M.M. Lerch, B. Brandt-Nedelev, W. Roth, M. Ruthenbuerger, T. Reinheckel, W. Domschke, H. Lippert, C. Peters, and J. Deussing. 2000. Role of cathepsin B in intracellular trypsinogen activation and the onset of acute pancreatitis. *J. Clin. Invest.* 106:773–781. http://dx.doi.org/10.1172/JCI9411

Hall, J.D., M.D. Woolard, B.M. Gunn, R.R. Craven, S. Taft-Benz, J.A. Frelinger, and T.H. Kawula. 2008. Infected-host-cell repertoire and cellular response in the lung following inhalation of *Francisella tularensis* Schu S4, LVS, or U112. *Infect. Immun.* 76:5843–5852. http://dx.doi.org/10.1128/IAI.01176-08

Halle, A., V. Hornung, G.C. Petzold, C.R. Stewart, B.G. Monks, T. Reinheckel, K.A. Fitzgerald, E. Latz, K.J. Moore, and D.T. Golenbock. 2008. The NALP3 inflammasome is involved in the innate immune response to amyloid-β. *Nat. Immunol.* 9:857–865. http://dx.doi.org/10.1038/ni.1636

Henry, T., A. Brotcke, D.S. Weiss, L.J. Thompson, and D.M. Monack. 2007. Type I interferon signaling is required for activation of the inflammasome during *Francisella* infection. *J. Exp. Med.* 204:987–994. http://dx.doi.org/10.1084/jem.20062665

Huang, J., and J.H. Brumell. 2014. Bacteria-autophagy interplay: a battle for survival. *Nat. Rev. Microbiol.* 12:101–114. http://dx.doi.org/10.1038/nrmicro3160

Irizarry, R.A., B. Hobbs, F. Collin, Y.D. Beazer-Barclay, K.J. Antonellis, U. Scherf, and T.P. Speed. 2003. Exploration, normalization, and summaries of high density oligonucleotide array probe level data. *Biostatistics.* 4:249–264. http://dx.doi.org/10.1093/biostatistics/4.2.249

Jones, J.W., N. Kayagaki, P. Broz, T. Henry, K. Newton, K. O'Rourke, S. Chan, J. Dong, Y. Qu, M. Roose-Girma, et al. 2010. Absent in melanoma 2 is required for innate immune recognition of *Francisella tularensis*. *Proc. Natl. Acad. Sci. USA.* 107:9771–9776. http://dx.doi.org/10.1073/pnas.1003738107

Kanistanon, D., D.A. Powell, A.M. Hajjar, M.R. Pelletier, I.E. Cohen, S.S. Way, S.J. Skerrett, X. Wang, C.R. Raetz, and R.K. Ernst. 2012. Role of *Francisella* lipid A phosphate modification in virulence and long-term protective immune responses. *Infect. Immun.* 80:943–951. http://dx.doi.org/10.1128/IAI.06109-11

Karki, R., S.M. Man, R.K. Malireddi, P. Gurung, P. Vogel, M. Lamkanfi, and T.D. Kanneganti. 2015. Concerted activation of the AIM2 and NLRP3 inflammasomes orchestrates host protection against *Aspergillus* infection. *Cell Host Microbe.* 17:357–368. http://dx.doi.org/10.1016/j.chom.2015.01.006

Kessenbrock, K., L. Fröhlich, M. Sixt, T. Lämmermann, H. Pfister, A. Bateman, A. Belaaouaj, J. Ring, M. Ollert, R. Fässler, and D.E. Jenne. 2008. Proteinase 3 and neutrophil elastase enhance inflammation in mice by inactivating antiinflammatory progranulin. *J. Clin. Invest.* 118:2438–2447.

Kim, J., M. Kundu, B. Viollet, and K.-L. Guan. 2011. AMPK and mTOR regulate autophagy through direct phosphorylation of Ulk1. *Nat. Cell Biol.* 13:132–141. http://dx.doi.org/10.1038/ncb2152

Kiselyov, K., J. Chen, Y. Rbaibi, D. Oberdick, S. Tjon-Kon-Sang, N. Shcheynikov, S. Muallem, and A. Soyombo. 2005. TRP-ML1 is a lysosomal monovalent cation channel that undergoes proteolytic cleavage. *J. Biol. Chem.* 280:43218–43223. http://dx.doi.org/10.1074/jbc.M508210200

Kreuzaler, P.A., A.D. Staniszewska, W. Li, N. Omidvar, B. Kedjouar, J. Turkson, V. Poli, R.A. Flavell, R.W.E. Clarkson, and C.J. Watson. 2011. Stat3 controls lysosomal-mediated cell death in vivo. *Nat. Cell Biol.* 13:303–309. http://dx.doi.org/10.1038/ncb2171

Lindgren, H., L. Stenman, A. Tärnvik, and A. Sjöstedt. 2005. The contribution of reactive nitrogen and oxygen species to the killing of *Francisella tularensis* LVS by murine macrophages. *Microbes Infect.* 7:467–475. http://dx.doi.org/10.1016/j.micinf.2004.11.020

Luzio, J.P., P.R. Pryor, and N.A. Bright. 2007. Lysosomes: fusion and function. *Nat. Rev. Mol. Cell Biol.* 8:622–632. http://dx.doi.org/10.1038/nrm2217

MacIvor, D.M., S.D. Shapiro, C.T. Pham, A. Belaaouaj, S.N. Abraham, and T.J. Ley. 1999. Normal neutrophil function in cathepsin G-deficient mice. *Blood.* 94:4282–4293.

Man, S.M., and T.D. Kanneganti. 2015. Regulation of inflammasome activation. *Immunol. Rev.* 265:6–21. http://dx.doi.org/10.1111/imr.12296

Man, S.M., and T.D. Kanneganti. 2016. Converging roles of caspases in inflammasome activation, cell death and innate immunity. *Nat. Rev. Immunol.* 16:7–21. http://dx.doi.org/10.1038/nri.2015.7

Man, S.M., R. Karki, R.K. Malireddi, G. Neale, P. Vogel, M. Yamamoto, M. Lamkanfi, and T.D. Kanneganti. 2015. The transcription factor IRF1 and guanylate-binding proteins target activation of the AIM2 inflammasome by *Francisella* infection. *Nat. Immunol.* 16:467–475. http://dx.doi.org/10.1038/ni.3118

Man, S.M., R. Karki, and T.D. Kanneganti. 2016. AIM2 inflammasome in infection, cancer, and autoimmunity: Role in DNA sensing, inflammation, and innate immunity. *Eur. J. Immunol.* 46:269–280. http://dx.doi.org/10.1002/eji.201545839

Martinez, J., J. Almendinger, A. Oberst, R. Ness, C.P. Dillon, P. Fitzgerald, M.O. Hengartner, and D.R. Green. 2011. Microtubule-associated protein 1 light chain 3 alpha (LC3)-associated phagocytosis is required for the efficient clearance of dead cells. *Proc. Natl. Acad. Sci. USA.* 108:17396–17401. http://dx.doi.org/10.1073/pnas.1113421108

Medina, D.L., S. Di Paola, I. Peluso, A. Armani, D. De Stefani, R. Venditti, S. Montefusco, A. Scotto-Rosato, C. Prezioso, A. Forrester, et al. 2015. Lysosomal calcium signalling regulates autophagy through calcineurin and TFEB. *Nat. Cell Biol.* 17:288–299. http://dx.doi.org/10.1038/ncb3114

Meunier, E., P. Wallet, R.F. Dreier, S. Costanzo, L. Anton, S. Rühl, S. Dussurgey, M.S. Dick, A. Kistner, M. Rigard, et al. 2015. Guanylate-binding proteins promote activation of the AIM2 inflammasome during infection with *Francisella novicida*. *Nat. Immunol.* 16:476–484. http://dx.doi.org/10.1038/ni.3119

Miao, Y., G. Li, X. Zhang, H. Xu, and S.N. Abraham. 2015. A TRP channel senses lysosome neutralization by pathogens to trigger their expulsion. *Cell.* 161:1306–1319. http://dx.doi.org/10.1016/j.cell.2015.05.009

Miller, A., J. Schafer, C. Upchurch, E. Spooner, J. Huynh, S. Hernandez, B. McLaughlin, L. Oden, and H. Fares. 2015. Mucolipidosis type IV protein TRPML1-dependent lysosome formation. *Traffic.* 16:284–297. http://dx.doi.org/10.1111/tra.12249

Mueller-Steiner, S., Y. Zhou, H. Arai, E.D. Roberson, B. Sun, J. Chen, X. Wang, G. Yu, L. Esposito, L. Mucke, and L. Gan. 2006. Antiamyloidogenic and neuroprotective functions of cathepsin B: implications for Alzheimer's disease. *Neuron.* 51:703–714. http://dx.doi.org/10.1016/j.neuron.2006.07.027

Nano, F.E., N. Zhang, S.C. Cowley, K.E. Klose, K.K. Cheung, M.J. Roberts, J.S. Ludu, G.W. Letendre, A.I. Meierovics, G. Stephens, and K.L. Elkins. 2004. A *Francisella tularensis* pathogenicity island required for intramacrophage growth. *J. Bacteriol.* 186:6430–6436. http://dx.doi.org/10.1128/JB.186.19.6430-6436.2004

Palm, W., Y. Park, K. Wright, N.N. Pavlova, D.A. Tuveson, and C.B. Thompson. 2015. The utilization of extracellular proteins as nutrients is suppressed by mTORC1. *Cell.* 162:259–270. http://dx.doi.org/10.1016/j.cell.2015.06.017

Palmieri, M., S. Impey, H. Kang, A. di Ronza, C. Pelz, M. Sardiello, and A. Ballabio. 2011. Characterization of the CLEAR network reveals an integrated control of cellular clearance pathways. *Hum. Mol. Genet.* 20:3852–3866. http://dx.doi.org/10.1093/hmg/ddr306

Perera, R.M., S. Stoykova, B.N. Nicolay, K.N. Ross, J. Fitamant, M. Boukhali, J. Lengrand, V. Deshpande, M.K. Selig, C.R. Ferrone, et al. 2015. Transcriptional control of autophagy-lysosome function drives pancreatic cancer metabolism. *Nature.* 524:361–365. http://dx.doi.org/10.1038/nature14587

Rathinam, V.A., Z. Jiang, S.N. Waggoner, S. Sharma, L.E. Cole, L. Waggoner, S.K. Vanaja, B.G. Monks, S. Ganesan, E. Latz, et al. 2010. The AIM2 inflammasome is essential for host defense against cytosolic bacteria and DNA viruses. *Nat. Immunol.* 11:395–402. http://dx.doi.org/10.1038/ni.1864

Ray, K., B. Marteyn, P.J. Sansonetti, and C.M. Tang. 2009. Life on the inside: the intracellular lifestyle of cytosolic bacteria. *Nat. Rev. Microbiol.* 7:333–340. http://dx.doi.org/10.1038/nrmicro2112

Roy, C.R., S.P. Salcedo, and J.P. Gorvel. 2006. Pathogen-endoplasmic-reticulum interactions: in through the out door. *Nat. Rev. Immunol.* 6:136–147. http://dx.doi.org/10.1038/nri1775

Samie, M., and P. Cresswell. 2015. The transcription factor TFEB acts as a molecular switch that regulates exogenous antigen-presentation pathways. *Nat. Immunol.* 16:729–736. http://dx.doi.org/10.1038/ni.3196

Santic, M., M. Molmeret, and Y. Abu Kwaik. 2005. Modulation of biogenesis of the *Francisella tularensis* subsp. *novicida*-containing phagosome in quiescent human macrophages and its maturation into a phagolysosome upon activation by IFN-γ. *Cell. Microbiol.* 7:957–967. http://dx.doi.org/10.1111/j.1462-5822.2005.00529.x

Sardiello, M., M. Palmieri, A. di Ronza, D.L. Medina, M. Valenza, V.A. Gennarino, C. Di Malta, F. Donaudy, V. Embrione, R.S. Polishchuk, et al. 2009. A gene network regulating lysosomal biogenesis and function. *Science.* 325:473–477.

Settembre, C., C. Di Malta, V.A. Polito, M. Garcia Arencibia, F. Vetrini, S. Erdin, S.U. Erdin, T. Huynh, D. Medina, P. Colella, et al. 2011. TFEB links autophagy to lysosomal biogenesis. *Science.* 332:1429–1433. http://dx.doi.org/10.1126/science.1204592

Settembre, C., R. Zoncu, D.L. Medina, F. Vetrini, S. Erdin, S. Erdin, T. Huynh, M. Ferron, G. Karsenty, M.C. Vellard, et al. 2012. A lysosome-to-nucleus signalling mechanism senses and regulates the lysosome via mTOR and TFEB. *EMBO J.* 31:1095–1108. http://dx.doi.org/10.1038/emboj.2012.32

Settembre, C., A. Fraldi, D.L. Medina, and A. Ballabio. 2013. Signals from the lysosome: a control centre for cellular clearance and energy metabolism. *Nat. Rev. Mol. Cell Biol.* 14:283–296. http://dx.doi.org/10.1038/nrm3565

Shen, D., X. Wang, X. Li, X. Zhang, Z. Yao, S. Dibble, X.P. Dong, T. Yu, A.P. Lieberman, H.D. Showalter, and H. Xu. 2012. Lipid storage disorders block lysosomal trafficking by inhibiting a TRP channel and lysosomal calcium release. *Nat. Commun.* 3:731. http://dx.doi.org/10.1038/ncomms1735

Steele, S., J. Brunton, B. Ziehr, S. Taft-Benz, N. Moorman, and T. Kawula. 2013. *Francisella tularensis* harvests nutrients derived via ATG5-independent autophagy to support intracellular growth. *PLoS Pathog.* 9:e1003562. http://dx.doi.org/10.1371/journal.ppat.1003562

Tschopp, J., and K. Schroder. 2010. NLRP3 inflammasome activation: The convergence of multiple signalling pathways on ROS production? *Nat. Rev. Immunol.* 10:210–215. http://dx.doi.org/10.1038/nri2725

Tsukuba, T., S. Yamamoto, M. Yanagawa, K. Okamoto, Y. Okamoto, K.I. Nakayama, T. Kadowaki, and K. Yamamoto. 2006. Cathepsin E–deficient mice show increased susceptibility to bacterial infection associated with the decreased expression of multiple cell surface Toll-like receptors. *J. Biochem.* 140:57–66. http://dx.doi.org/10.1093/jb/mvj132

van Acker, G.J.D., A.K. Saluja, L. Bhagat, V.P. Singh, A.M. Song, and M.L. Steer. 2002. Cathepsin B inhibition prevents trypsinogen activation and reduces pancreatitis severity. *Am. J. Physiol. Gastrointest. Liver Physiol.* 283:G794–G800. http://dx.doi.org/10.1152/ajpgi.00363.2001

Xu, H., and D. Ren. 2015. Lysosomal physiology. *Annu. Rev. Physiol.* 77:57–80. http://dx.doi.org/10.1146/annurev-physiol-021014-071649

Xu, X., J. Greenland, P. Baluk, A. Adams, O. Bose, D.M. McDonald, and G.H. Caughey. 2013. Cathepsin L protects mice from mycoplasmal infection and is essential for airway lymphangiogenesis. *Am. J. Respir. Cell Mol. Biol.* 49:437–444. http://dx.doi.org/10.1165/rcmb.2013-0016OC

Yu, L., C.K. McPhee, L. Zheng, G.A. Mardones, Y. Rong, J. Peng, N. Mi, Y. Zhao, Z. Liu, F. Wan, et al. 2010. Termination of autophagy and reformation of lysosomes regulated by mTOR. *Nature.* 465:942–946. http://dx.doi.org/10.1038/nature09076

Zhang, X., X. Li, and H. Xu. 2012. Phosphoinositide isoforms determine compartment-specific ion channel activity. *Proc. Natl. Acad. Sci. USA.* 109:11384–11389. http://dx.doi.org/10.1073/pnas.1202194109